Advanced NH_3 based absorption refrigeration cycles

Modelling of the ionic liquid based double-effect cycles

Bob Schouten
4051009

Technische Universiteit Delft

TU Delft Delft University of Technology

Challenge the future

Advanced NH_3 based absorption refrigeration cycles

Modelling of the ionic liquid based double-effect cycles

by

Bob Schouten

to obtain the degree of

Master of Science

in Mechanical Engineering at the Delft University of Technology, Process & Energy faculty, Energy Technology

Student number:	4051009
Supervisor:	Dr. ir. C.A. Infante Ferreira
Daily supervisor:	MSc. M. Wang, PhD candidate
Thesis committee:	Prof. dr. ir. T.J.H. Vlugt
	Dr. ir. C.A. Infante Ferreira
	Dr. ir. R.G. Hekkenberg
	MSc. M. Wang, PhD candidate

Preface

Firstly, I would like to thank my supervisor Dr. ir. C.A. Infante Ferreira for his continuous support and encouragement of my thesis project. His help and patience were very important during my graduation period.

I am also extremely thankful to my daily supervisor, MSc. Meng Wang, for helping me throughout the project. He was always there to give me feedback and help me with technical problems and writing my report.

Lastly, a special thanks goes to my family, my colleagues and of course my girlfriend, Shi-hsien, for their support.

Bob Schouten
Delft, June 2017

Abstract

Absorption refrigeration cycles are energy saving as they can be driven by waste heat instead of electricity. By doing so, they reduce the use of fossil fuels, resulting in a reduction of emissions. However, many challenges exist for the traditional working fluids of the cycle, such as the crystallization problem of the water-lithium bromide pair and the difficulty in separating ammonia from the ammonia-water working pair. Ionic liquids, as novel absorbents in absorption cycles, have attracted considerable attention because of their unique properties like negligible vapor pressure, negligible flammability, thermal stability, low melting temperatures, liquid state over a wide temperature range and good solubility.

In this thesis, a thermodynamic model of the ammonia based double-effect absorption cycle in series configuration was used to predict the performance and suitability of nine ionic liquids as potential absorbents. The performance of the ammonia-ionic liquid systems was compared with that of ammonia-water systems and the influence of the operating conditions and the design parameters on the performance was investigated.

Furthermore, a method to experimentally determine the excess enthalpy of ammonia and ionic liquid mixtures is proposed and the suitabilty of using absorption refrigeration on a fishing ship, with ionic liquids as absorbents, is studied.

The results show that the ionic liquids [Bmim][BF4], [Mmim][DMP] and [Emim][SCN] used as absorbents in the investigated absorption cycle reached the best performance and could be a promising replacement of water in the ammonia-water working pair. The best performing ionic liquid, [Bmim][BF4], was found to be a better performing absorbent than water in the double-effect cycle.

Contents

List of Tables

List of Figures

Nomenclature

Abbreviation

[Bmim][BF4]	1-butyl-3-methylimidazolium tetrafluoroborate
[Bmim][PF6]	1-butyl-3-methylimidazolium hexafluorophosphate
[Emim][BF4]	1-ethyl-3-methylimidazolium tetrafluoroborate
[Emim][EtOSO3]	1-ethyl-3-methylimidazolium ethylsulfate
[Emim][SCN]	1-ethyl-3-methylimidazolium thiocyanate
[Emim][Tf2N]	1-ethyl-3-methylimidazolium bis(trifluoromethylsulfonyl)imide
[Hmim][BF4]	1-methylimidazolium tetrafluoroborate
[Mmim][DMP]	1,3-dimethylimidazolium dimethyl phosphate
[Omim][BF4]	1-methyl-3-octylimidazolium tetrafluoroborate
ABS	Absorber
CON	Condenser
COP	Coefficient of performance
CWP	Chilled water plant
DSC	Differential scanning calorimeter
EOS	Equation of state
EVA	Evaporator
GAX	Generator absorber heat-exchange
HEX1	Heat exchanger 1
HEX2	Heat exchanger 2
HPC	High pressure condenser
HPG	High pressure generator
IPG	Intermediate pressure generator
NIST	National Institute of Standards and Technology
NRTL	Non random two liquid
REC1	Rectifier 1
REC2	Rectifier 2
RMSD	Root-mean-square deviation
RR	Reflux ratio

RSW	Refrigerated seawater
VLE	Vapor-liquid equilibrium

Symbol

ΔT	Temperature rise $[K]$
$\dot{m}$	Mass flow rate $[kg/s]$
$\dot{Q}$	Rate of heat transfer $[J/s]$
$\dot{W}$	Power $[J/s]$
c_p	Specific heat capacity $[J/kg/K]$
dT	Temperature difference between flows $[K]$
L	Length $[m]$
m	Mass $[kg]$
M^E	Excess property $[-]$
P	Pressure $[Pa]$
Q	Heat transfered $[J]$
T	Temperature $[K/°C]$
V	Volume $[m^3]$
x	Mass concentration of the refrigerant in the liquid phase $[kg/kg]$
y	Mass concentration of the refrigerant in the vapor phase $[kg/kg]$
$\bar{h}^E$	Specific mole based excess enthalpy $[J/mole]$
h^E	Specific mass based excess enthalpy $[J/kg]$
h	Specific mass based enthalpy $[J/kg]$

Super- and subscript

$1,2,...$	State indicator
$a,b,...$	Indicator of component in mixture
box	Experimental insulated box
$calc$	Calculated value
$cooling$	For a cooling application
dec	Decomposition
ex	Exhaust gas
exp	Experiment
$guess$	Guess value
H_2O	Water component
$heating$	For a heating application

i	Species of the i-t component
id	Ideal mixture
in	Inlet
l	Liquid phase
max	Maximum
min	Minimum
mix	Mixing
NH_3	Ammonia component
out	Outlet
$PUMP$	Solution pump
rec	Recovered
rel	Released
$samp$	Experimental connected sample
sat	Saturated condition
sea	Seawater
sol	Solution
tot	Total
v	Vapor phase
IL	Ionic liquid

Greek letter

α	Parameter in NRTL model [-]
γ	Activity coefficient [-]
τ	Parameter in NRTL model [-]
ρ	Density [kg/m^3]
η	Efficiency [−]

1 Introduction

1.1. Background

Nowadays, problems like global warming and pollution are increasingly standing out. The need for energy-saving and green technology is urgent. Absorption refrigeration and absorption heat pumps are energy-saving as they can be driven by solar power or waste heat making them promising technologies [30]. Additionally, they can use working fluids with zero "ozone depletion" and "global warming potential" fulfilling both the Montreal Protocol and the Kyoto Protocol [3]. Therefore, they have attracted much attention as a real alternative to traditional electricity consuming vapor-compression cycles [15, 40].

However, many challenges exist for the traditional working pairs, such as the crystallization problem of the water and lithium bromide pair when operating temperature is high and the difficulty in separating ammonia from the ammonia and water working pair [39]. New ionic liquids are being investigated for their potential roles in replacing the absorbents in traditional working pairs [1].

Ionic liquids are salts that remain in liquid state at near or below room temperature. In recent years, ionic liquids have attracted considerable attention because of their unique properties, e.g. negligible vapor pressure, negligible flammability, thermal stability, low melting temperatures, liquid state over a wide temperature range and good solubility [4, 6, 9, 27]. Therefore, absorption systems which make use of working pairs that include ionic liquids have been investigated.

Unfortunately, for the ammonia and ionic liquid systems, experimental heat capacity and mixing enthalpy data, which are critical for the evaluation of thermodynamic processes, have only scarcely been reported. Since ammonia based absorption systems are suitable for sub-zero degree applications and are free of air infiltration (they operate above atmospheric pressure), ammonia and ionic liquid working pairs could be very promising as working fluids for heat driven thermodynamic cycles.

1.2. Literature review

1.2.1. Absorption refrigeration and absorption heat pumps

Absorption technology, which is the focus of this thesis, is an example of a heat-driven technology. The simplest and most common heat-driven heat pump is a device that transfers heat at three temperature levels, as shown in figure 1.1. In this type of heat pump, the driving heat is delivered at the

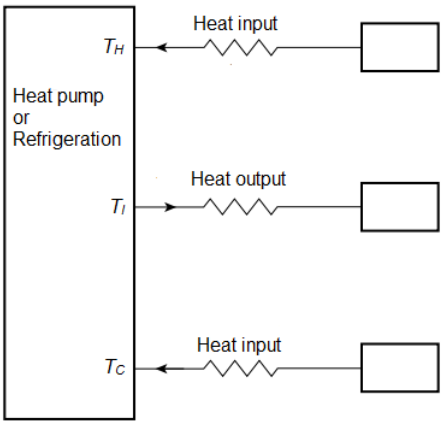

Figure 1.1: Temperature levels of a simple absorption heat pump or absorption refrigeration system. When the cycle is used for a cooling application, the cooling load is supplied at the lowest temperature level (T_C). For heating applications, the heat is delivered at the intermediate temperature level (T_I).

highest temperature level (T_H). The product is either refrigeration at the lowest temperature (T_C) or heating at the intermediate temperature (T_I). The single-effect absorption cycle is the most basic example operating at three temperature levels which is explained later in this section. Other heat-driven technologies that have been demonstrated include adsorption and Stirling cycle refrigeration [13].

Configurations of absorption cycles Absorption cycles have many different configurations including the single effect cycle, double effect cycle, double lift cycle, GAX cycle and other cycles [26]. Except for the single effect cycle, other cycles are proposed for high efficiency, high temperature lift or strong flexibility [35]. For example, the double effect cycle has a high COP, the double lift cycle has high temperature lift and the GAX cycle has stronger flexibility. All of the discussed configurations have an important feature in common, they all re-use heat within the cycle. This is referred to as "internal heat exchange". The most basic example of a device that utilizes internal heat is the solution heat exchanger. The single-effect cycle shown in figure 1.2 employs such a heat exchanger.

Single-effect absorption cycle Figure 1.2 shows the standard heat driven single effect absorption cycle (right) and the mechanical vapor-compression refrigeration cycle (left). They are two of the most basic and commonly used refrigeration cycles. Both the mechanical vapor-compression cycle and the absorption cycle make use of a condenser, valve and evaporator to supply the cooling power. However, the main difference between the two systems is the method used to compress the refrigerant vapor from the low pressure level to the high pressure level.

In the mechanical vapor compression refrigeration cycle a compressor is used to increase the pressure level of the refrigerant by using mechanical work, and thus, electricity. In contrast, with respect to the single-effect absorption cycle, the compressor is replaced by an absorber, generator, throttling valve and a solution pump. The combination of these components can be interpreted as a "thermal compressor" (see the dashed box in figure 1.2) as it uses heat as input instead of mechanical power to compress the refrigerant. Furthermore, a suitable working fluid that is able to absorb and desorb the refrigerant at certain temperatures and pressures is required to ensure effective operation.

During the thermal compression process, the refrigerant at the lowest pressure level coming from

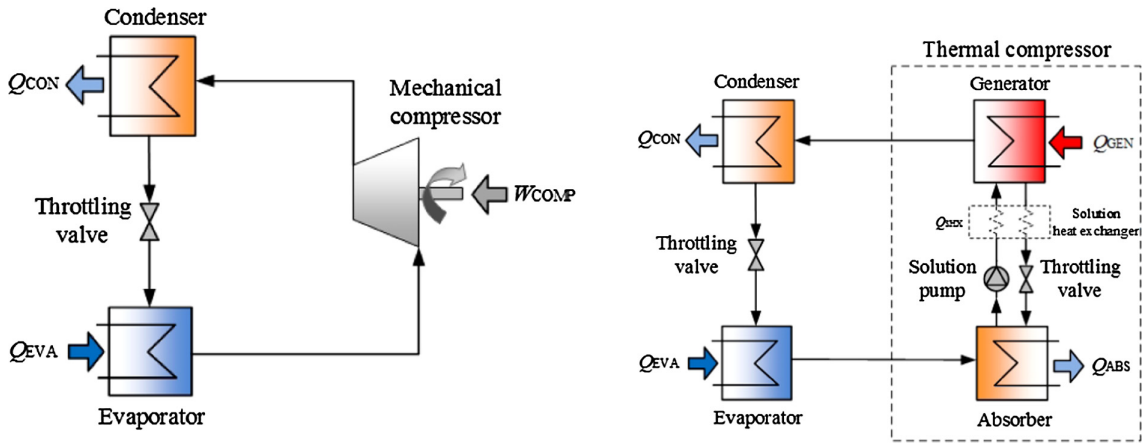

Figure 1.2: Left: mechanical vapor-compression refrigeration cycle, right: single effect absorption cycle. The two most basic refrigeration cycles. The mechanical vapor-compression cycle uses mechanical power, whereas the absorption cycle is driven by heat [8].

the evaporator enters the absorber where it is absorbed into a liquid solution to form a strong solution (strong in refrigerant). During this absorption process, the refrigerant condenses. After that, the strong solution is pumped from the low pressure level to the high pressure level after which it enters the generator, where the solution absorbs heat from a high temperature heat source to desorb the refrigerant. In most single-effect absorption cycles, a solution heat exchanger is deployed between the generator and the absorber in order to use the heat from the hot solution leaving the generator to pre-heat the cold solution coming from the absorber. By doing so, the solution heat exchanger reduces the heat required by the generator to desorb the refrigerant and the cooling power required by the absorber to condens and absorb the refrigerant. The major advantage of the thermal compressor compared to the mechanical compressor is that it needs much less mechanical power to boost the pressure of the refrigerant. Instead of mechanical power, the thermal compressor uses a heat input in the generator from a temperature that is greater than the ambient temperature. Single effect absorption chillers are marketed products. Companies including Broad, Carrier, Colibri, Mitsubishi, Robur, Sanyo, Trane, York and some other companies all have business on single-effect water–lithium bromide chillers or single-effect ammonia– water chillers [13].

Double-effect effect absorption cycle The single-effect absorption system has a relatively low COP due to which it is not competing economically with the conventional vapor compression system, except in case of waste heat applications where the input energy is virtually free of cost. To reduce operating cost of the absorption cycle, it is desirable to increase the COP. Therefore, multi-effect absorption systems with high temperature heat sources have now been developed [2].

Figure 1.3 shows a simplified process flow diagram of a double-effect absorption cycle in series configuration. The cycle makes use of "internal heat exchange" in a couple of ways. The condensation–generation coupling increases the cycle efficiency by using condensation heat from the vapor in the high pressure condenser to generate vapor in the intermediate pressure generator. At the same time, the driving temperature and system pressure are increased.

When the heat source temperature increases, the COP of a single effect cycle only stays stable. In order to make better use of the heat input, the condensation–generation heat coupling is used to form a new cycle, as shown in figure 1.3 in the dashed box.

Series, parallel or reverse configurations can be adopted for the solution flow. In the series flow configuration, the solution from the absorber flows into the high pressure generator and intermediate

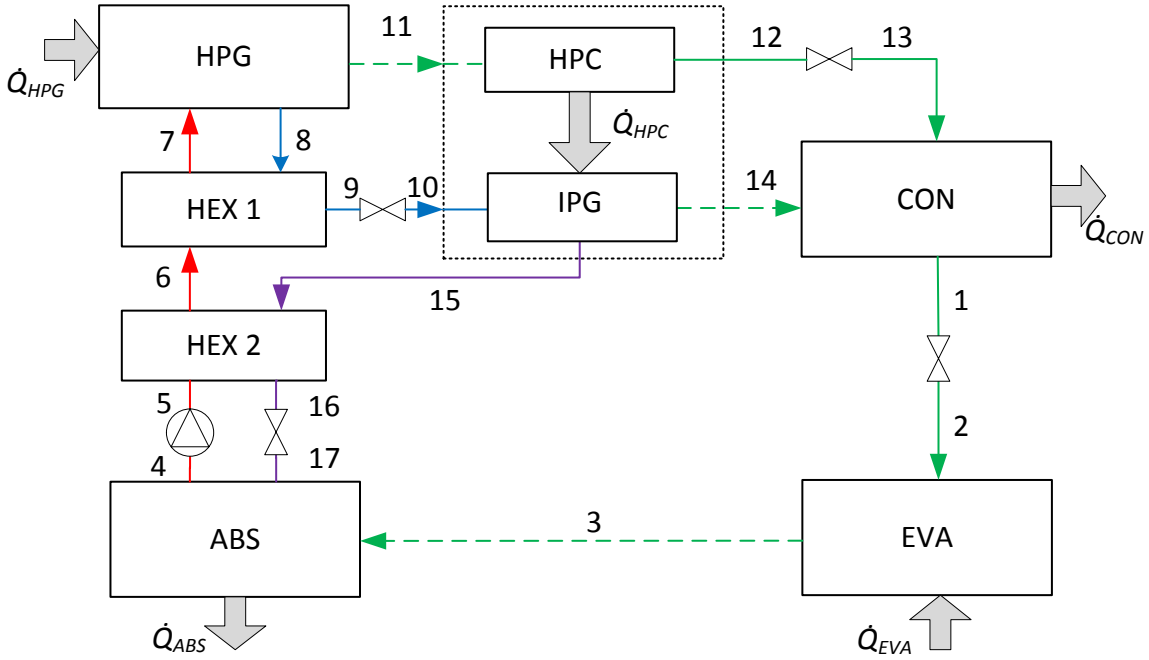

Figure 1.3: Process flow diagram of the double-effect absorption cycle in a series configuration. The red, blue and purple lines indicate the strong, intermediate and weak solution flows respectively. The green lines indicate the refrigerant flow. The dotted lines indicate the vapor phase and the solid lines indicate the liquid phase.

pressure generator successively. In the parallel flow configuration, the solution from the absorber flows into the high pressure generator and the intermediate pressure generator at the same time. In the reverse flow configuration, the solution from the absorber first flows into the intermediate pressure generator and then into the high pressure generator [35].

Herold et al. [13] presented the cooling capacities of different solution flow configurations for the double-effect absorption cycle from simulation. The cooling capacities of series, parallel and reverse configurations were investigated and series flow was found to have the highest capacity. Because of this, series flow will be investigated in present research.

Traditional working pairs The most common working pairs for absorption systems are lithium bromide-water and ammonia-water. Lithium bromide–water based absorption systems are widely used for their high efficiency. This working pair utilizes water as refrigerant and is therefore limited to evaporation temperatures above 0 °C. Absorption cycles based on this working pair are typically configured as water chillers for air-conditioning systems in large buildings. They have a reputation as consistent and dependable. The COP typically varies over the range $0.7 < COP < 1.2$. Single effect lithium bromide–water systems are manufactured and sold throughout the world. Single-effect machines are typically fired indirectly with heat coming from steam or hot water at temperatures above 75 °C and with COPs around 0.7. Double-effect lithium bromide-water systems are also manufactured by multiple companies. The COP of these double-effect systems typically varies from 1.0 to 1.2 [13].

The ammonia–water absorption chiller is popular for no danger of crystallization and the ice-making ability. Besides, the wide concentration range of ammonia–water allows heat recovery through

generator-absorber heat exchange (GAX). This working pair utilizes ammonia as the refrigerant. One advantage of ammonia as refrigerant is that the allowable refrigeration temperature is very low (the freezing temperature of ammonia is -77.7 °C). Single-stage ammonia-water systems have been in use for a long time [13].

Ammonia is a colorless gas of low density (lower than air) at room temperature with a pungent smell. It is widely used for agriculture as fertilizer and source material for fibers, plastics, explosives and cleaning agents. It can be transported as a liquid under a pressure of 1 MPa and at 25 °C. The critical point of ammonia is at 132.2 °C and 11.3 MPa. The strong odor can be seen as an asset. Even very small leaks are easily noticed and therefore a significant incentive exists for early repairs and consistent maintenance. Compared to lithium bromide-water systems, operating pressures are higher. This is because the boiling point at atmospheric pressure of ammonia is -33.35 °C, compared to 100°C for water. A second important difference is that the vapor pressure of water (the absorbent) is not negligible relative to that of ammonia. As a consequence, vapor generated in the generator contains a certain amount of water. Any water contained in the vapor leaving the generator is harmful to the performance of the system. The water will pass with the vapor into the condenser and then into the evaporator where the water tends to accumulate. Accumulation of water in the evaporator will lead to a decrease in evaporator pressure which in turn, affects the absorber conditions because they operate at the same pressure. One way of preventing excessive water accumulation in the evaporator is to drain it into the absorber. However this method harms the performance of the system in two ways. First, the water was evaporated in the generator, requiring heat input, but it does not evaporate in the evaporator, so it does not provide cooling capacity. Second, the water accumulated in the evaporator contains an amount of ammonia that is, consequently, not evaporated amplifying this effect. To prevent this, a rectifier can be added. Figure 1.4 shows a single-effect cycle that employs a rectifier. The water containing vapor leaves the desorber (generator) and flows into the rectifier. The rectifier exchanges heat with the environment cooling down the vapor, causing most of the water to condens. The water will flow back into the generator as reflux preventing the accumulation of water in the evaporator. Because of this undesired evaporated water, the generator requires more heat input which decreases the performance.

Concluding, for the same application, lithium bromide-water is more efficient than ammonia-water. The reasons are hidden in the fluid properties. As explained before, because ammonia-water needs a rectifier the efficiency goes down. Furthermore, the specific heat of ammonia-water is about twice as large as lithium bromide-water. Thus, any inefficiency of the solution heat exchangers causes a large penalty in ammonia-water systems. Lastly, the latent heat of ammonia is about half as large as that of water. Thus, for the same cooling capacity in the evaporator, a larger refrigerant flow is required.

1.2.2. Methods to measure excess enthalpies

Diffusivities, heat capacities and solubilities of various ionic liquid mixtures have been studied [1, 4, 6, 9, 27, 29]. Then, very high solubilities were found which led researchers to think of several applications with ionic liquid mixtures. One of the proposed applications was for absorption cycles. The feasibility of ammonia absorption cycles, using ionic liquids as absorbents, was investigated and very high solubilities were found [37]. Also the experimental PTx-data have successfully been correlated with an equation of state (EOS) model which has been used to calculate excess properties [36]. According to that study, the properties of the ammonia ionic liquid mixtures show promise for replacing the traditional ammonia water working pair for absorption cycle applications.

Different methods have been demonstrated for measuring various properties of ionic liquid mixtures. Excess enthalpies of ionic liquids with short-chain alcohols, e.g. ethanol and propanol, have

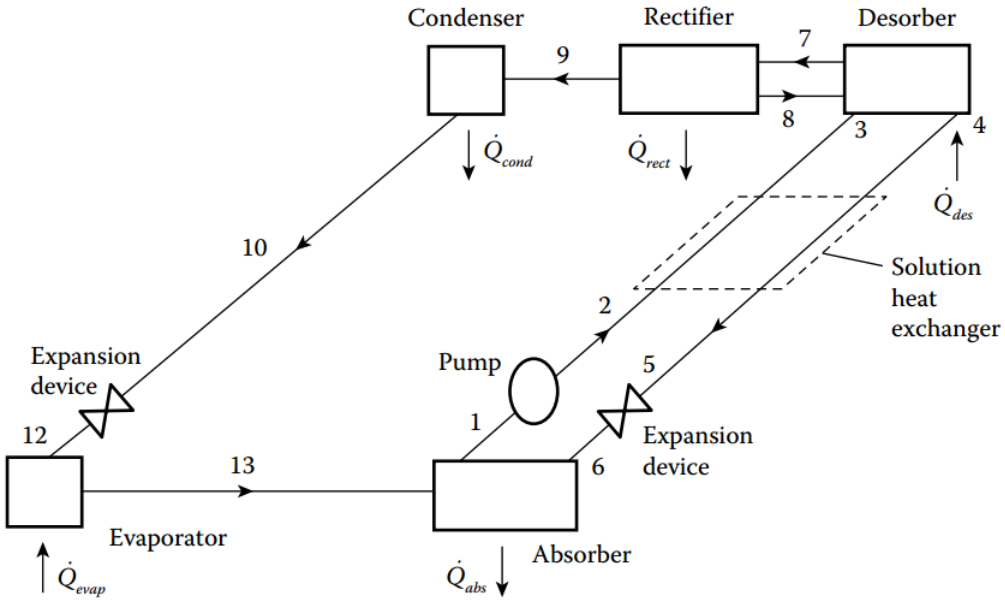

Figure 1.4: Single-effect absorption cycle using a rectifier. The rectifier is used to remove water from the vapor steam leaving the desorber in order to prevent water accumulation in the evaporator [13].

been measured using isothermal titration calorimetry [23]. Other methods include the use of static phase equilibrium cells [36]. It is important to know whether mixing processes between ammonia and water are exothermic, because this is a necessary property for the absorption cycle.

1.3. Research objectives

The main objective of this thesis is to analyze the performance of the double-effect absorption cycle in series configuration using ionic liquid-ammonia working pairs and to compare them with the ammonia-water working pair. Further objectives are to develop a method to experimentally determine the mixing enthalpy of ammonia ionic liquid mixtures and to investigate the suitability of absorption refrigeration, using an ionic liquid as absorbent, on a fishing ship for the refrigeration of fish.

1.4. Thesis outline

- Chapter 2 describes the thermodynamic model of a double-effect absorption cycle with two rectifiers in series configuration with ammonia and water as working pair. The influence of the operating conditions and the design parameters is investigated.
- Chapter 3 uses the thermodynamic model described in chapter 2, without the rectifiers, to predict the performance and suitability of nine ionic liquids as absorbents using ammonia as refrigerant.
- Chapter 4 proposes a method to measure the mixing enthalpy of ammonia and ionic liquid mixtures using samples.
- Chapter 5 describes a case-study of a Dutch trawler fishing vessel and the opportunity to use

[Bmim][BF4] and ammonia as working pair for the double-effect absorption cycle on board for the refrigeration fish.

- Chapter 6 presents the conclusions and outlook

2

Double-Effect absorption system with ammonia-water

2.1. Introduction

This chapter describes the mathematical model to calculate thermodynamic processes of a double-effect absorption cycle using ammonia and water as working pair. The performance and limitations of the cycle under different operating conditions are investigated. A modification of the model is used in chapter 3 to do the same investigation for ammonia and ionic liquid working pairs. Firstly, the thermodynamic model of the double-effect ammonia-water absorption cycle in series configuration will be described in detail. The boundaries, the individual components within the system, the assumptions of the model, and the formulation of the mathematical equations are presented. Then, the results obtained by the thermodynamic model are discussed and the behaviour of the model is analysed. Lastly, the influence of the design parameters on the performance of the cycle is investigated and the conclusions are presented.

2.2. Thermodynamic model

2.2.1. Cycle description

A process flow diagram of the double effect absorption cycle in series configuration is shown in figure 2.1. The main components of this cycle are the high pressure generator (HPG), the intermediate pressure generator (IPG), the high pressure condenser (HPC), the condenser (CON), the absorber (ABS), the evaporator (EVA), two rectifiers (REC1 and REC2) and two solution heat exchangers (HEX1 and HEX2). The main difference with a traditional double effect series cycle is the addition of two rectifiers because the ammonia rich vapor coming from the high pressure generator and the intermediate pressure generator (streams 11a and 14a) has to be purified. If these streams do not get purified, water may build up in the evaporator which could cause the system to fail.

A qualitative illustration of the temperature and pressure relationship of each state is illustrated in figure 2.2. The diagram shows the relation between the three pressure levels and temperatures in the evaporator, absorber, condenser and high pressure generator. The diagonal lines are constant concentration lines. The lowest pressure level (P_{EVA}) is determined by the evaporation temperature of the pure ammonia, which is displayed by the green diagonal line. The strongest solution concentration (x_4) is determined by the intersection between the absorber outlet temperature and the lowest pressure level.

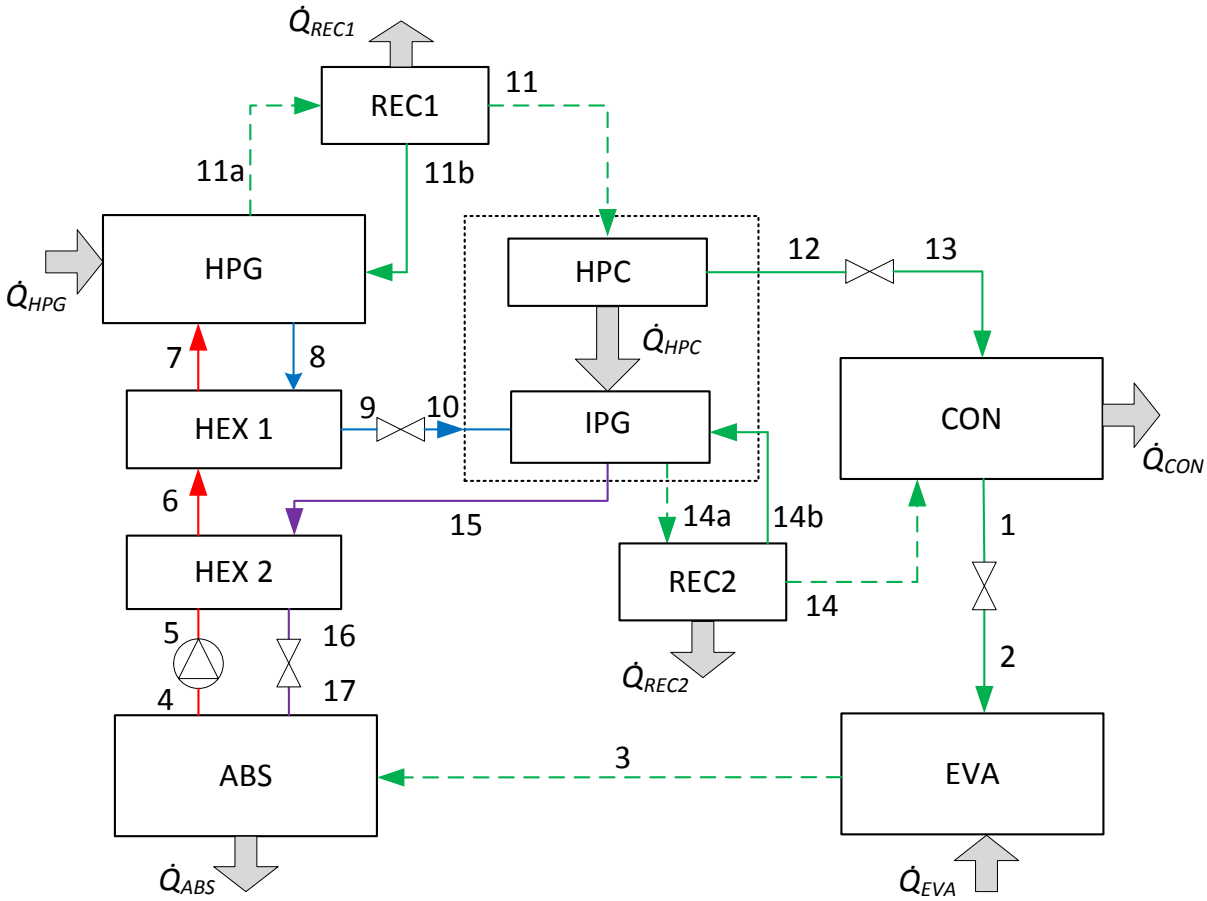

Figure 2.1: Process flow diagram of the double-effect absorption cycle in a series configuration. The red, blue and purple lines indicate the solution of the weak, intermediate and strong concentration. Green lines indicate the refrigerant flows. The dotted lines indicate the vapor phase and the solid lines indicate the liquid phase. The grey arrows indicate where the exchange of heat takes place.

Figure 2.3 shows how the double-effect absorption cycle interacts with the environment when it is used for a cooling application, for example making ice or the air conditioning of a building. The cooling demand ($\dot{Q}_{EVA}$) is supplied by the evaporator, where ammonia gets evaporated at the lowest pressure (P_{EVA}) and temperature level (T_{EVA}). The absorber rejects heat to the environment ($\dot{Q}_{ABS}$) to condens ammonia and absorb it into the solution. Similarly, the condenser rejects heat to the environment while condensing ammonia at the intermediate pressure level (P_{CON}). Usually, the absorber and condenser exchange heat with water or air from the environment at ambient temperature. At the highest pressure level (P_{HPG}), the high pressure generator absorbs heat ($\dot{Q}_{HPG}$) from an external source to evaporate ammonia from the solution. Furthermore, the pump uses power ($\dot{W}_{PUMP}$) to pump the solution around. To study the performance of the cycle during a cooling application the coefficient of performance (COP) is used which can be calculated with equation 2.1.

$$COP_{cool} = \frac{\dot{Q}_{EVA}}{\dot{Q}_{HPG} + \dot{W}_{PUMP}} \tag{2.1}$$

Figure 2.4 shows how the cycle interacts with the environment when it is used for a heating application. The heating of the application, for example the heating of a building, takes place at multiple components. Because the ammonia vapor leaving the low and high pressure generators has to be

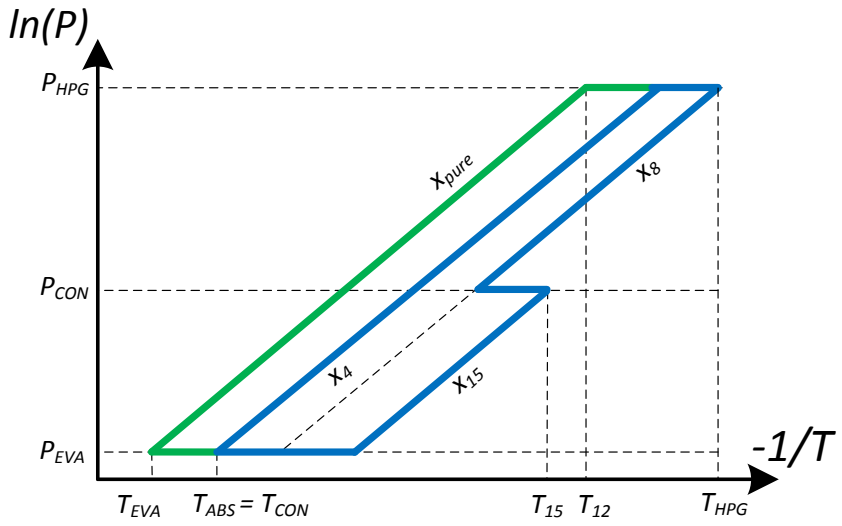

Figure 2.2: The double effect absorption cycle in a qualitative P-T-x diagram. The diagram shows the relation between the three pressure levels and temperatures in the evaporator, absorber, condenser and high pressure generator. The diagonal lines are constant concentration lines. The pure ammonia line is green and the solution concentration lines are blue.

rectified, more heat is rejected to the environment. This extra heat can be used to increase the performance. The COP of the cycle when it used for a heating application is calculated with equation 2.2.

$$COP_{heat} = \frac{\dot{Q}_{ABS} + \dot{Q}_{CON} + \dot{Q}_{REC1} + \dot{Q}_{REC2}}{\dot{Q}_{HPG} + W_{PUMP}} \tag{2.2}$$

In order to represent and simplify the physics of the double-effect absorption cycle, the following assumptions are made:

- The system operates at steady state
- The pressure drop due to friction in the pipelines and the heat exchangers of the system is negligible
- All components are well insulated and the heat losses to the surrounding are negligible
- The refrigerant at the outlet of the condenser is saturated liquid
- The solution at the outlet of the evaporator is saturated vapor
- At the exit of the absorber and the generators, the solutions are at equilibrium conditions
- The vapor outlets of the rectifiers are 30 K superheated
- The solution outlets of the rectifiers are at saturation conditions, 20 K lower than the vapor outlet temperatures.
- The vapor outlets of the rectifiers have a minimum purity of 99.9%
- The vapor outlets of the high pressure generator and the intermediate pressure generator have the same temperature as the respective strong solution inlet
- The pinch temperatures of HEX1, HEX2 and the intermediate pressure generator are 5 K

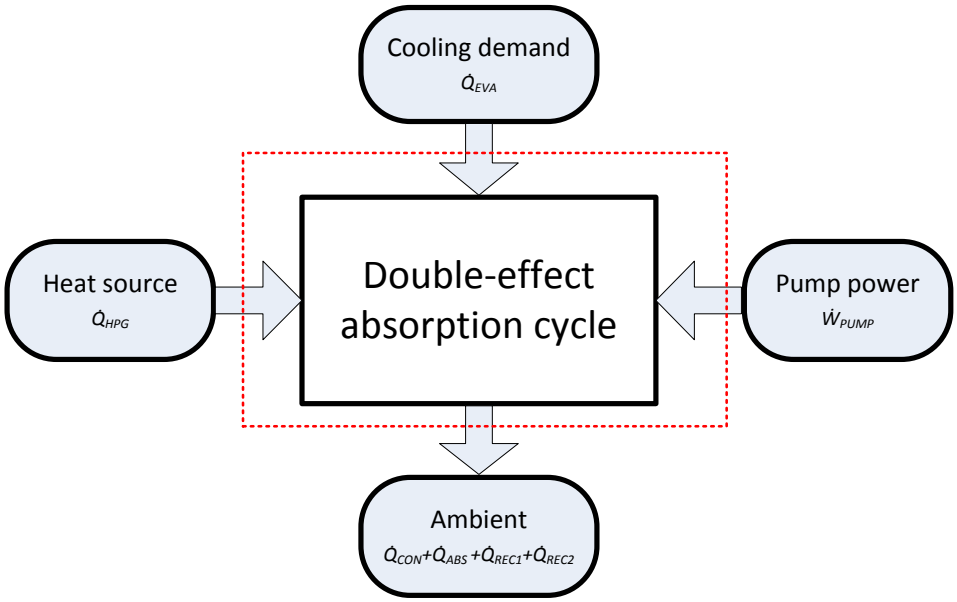

Figure 2.3: Boundary of the double effect absorption system when it is used for cooling. The red dotted line displays the boundary of the system, the heat flows and power demand used to calculate the COP are displayed for the different components.

The cycle operates at three different pressure levels, as can be seen figure 2.2. These can be determined by using the operating conditions T_{EVA}, T_{ABS}, T_{CON} and T_{HPG}. The absorber and the evaporator operate at the lowest pressure level P_{EVA}. This pressure level can be determined by the temperature of the evaporator because we know the composition of the saturated stream leaving the evaporator. With these properties the pressure can be determined from NIST's REFPROP database [17]. The condenser and second rectifier operate at the intermediate pressure level P_{CON}. This pressure level can be determined from the condenser temperature T_{CON} and the composition which has been imposed. With P_{EVA} and T_{ABS} the concentration of the ammonia rich stream leaving the absorber can be determined. This concentration remains unchanged until it reaches the high pressure generator.

The highest pressure level, P_{HPG}, is determined by the outlet temperature (T_{12}) of the intermediate pressure generator. With P_{HPG} and T_{HPG} the concentration of the ammonia lean solution leaving the high pressure generator can be determined giving the concentration of state points 8, 9 and 10. To calculate all the other points, heat balances, mass balances and species balances are used. These balances are calculated for each component as follows:

Solution pump To calculate the work done by the pump we assume a pump efficiency η_{PUMP} and use the following equations. A mass flow of 1 kg/s is assumed, this can always be changed to match the desired heating or cooling demand.

$$\dot{m}_4 = \dot{m}_5 \tag{2.3}$$

$$\dot{W}_{pump} = \frac{\dot{m}_5}{\rho_{sol}} \frac{P_{HPG} - P_{EVA}}{\eta_{PUMP}} \tag{2.4}$$

High pressure generator and the first rectifier Heat is supplied to the high pressure generator in order to evaporate ammonia from the solution. This vapor goes to the rectifier which sends a part of this back to the high pressure generator as reflux. The ammonia lean solution exits the high

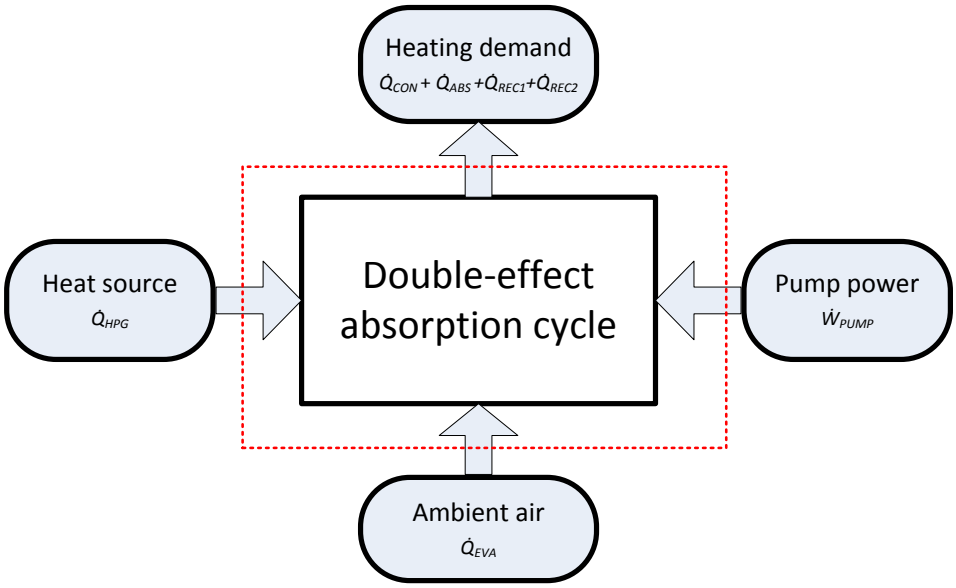

Figure 2.4: Boundary of the double effect absorption system when it is used for heating. The red dotted line displays the boundary of the system, the heat flows and power demand used to calculate the COP are displayed for the different components

pressure generator and goes to the first solution heat exchanger. The balances for the high pressure generator are as follows:

$$\dot{m}_7 + \dot{m}_{11b} = \dot{m}_{11a} + \dot{m}_8 \tag{2.5}$$

$$x_7\dot{m}_7 + x_{11b}\dot{m}_{11b} = y_{11a}\dot{m}_{11a} + x_8\dot{m}_8 \tag{2.6}$$

$$\dot{Q}_{HPG} = \dot{m}_{11a}h_{11a} + \dot{m}_8h_8 - \dot{m}_7h_7 - \dot{m}_{11b}h_{11b} \tag{2.7}$$

The vapor coming from the high pressure generator is cooled down in the rectifier to increase the quality of the vapor. The balances are as follows:

$$\dot{m}_{11a} = \dot{m}_{11b} + \dot{m}_{11} \tag{2.8}$$

$$y_{11a}\dot{m}_{11a} = x_{11b}\dot{m}_{11b} + y_{11}\dot{m}_{11} \tag{2.9}$$

$$\dot{Q}_{REC1} = \dot{m}_{11a}h_{11a} - \dot{m}_{11b}h_{11b} - \dot{m}_{11}h_{11} \tag{2.10}$$

A physical interpretation of the high pressure generator and rectifier is shown in figure 2.5. For working pairs with an absorbent with non-negligible vapor pressure, like ammonia-water, this purification section is needed. Stream 11a and stream 7 are in equilibrium. Furthermore, the following assumptions apply:

$$T_{11} = T_{12} + 30K \tag{2.11}$$

$$T_{11b} = T_{11} - 20K \tag{2.12}$$

The reflux ratio is calculated as follows:

$$RR_{REC1} = \frac{m_{11b}}{m_{11}} = \frac{y_{11a} - y_{11}}{x_{11b} - y_{11a}} \tag{2.13}$$

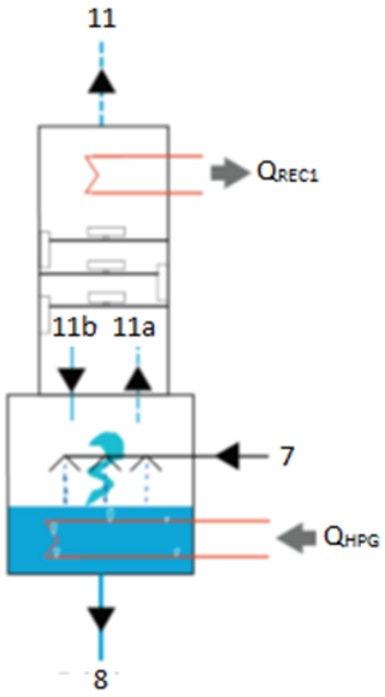

Figure 2.5: A schematic illustration of a generator with a rectifier on top. This set-up can be used for working pairs using absorbents with a volatile absorbent, like ammonia-water in this study. The incoming and outgoing fluid and heat flows are displayed for the high pressure generator and the first rectifier [16].

Intermediate pressure generator, high pressure condenser and the second rectifier Saturated vapor from the high pressure generator (stream 11) is condensed in the high pressure condenser and the heat that is rejected ($\dot{Q}_{HPC}$) is used to evaporate more ammonia coming from the first heat exchanger (stream 10). The intermediate pressure generator has a similar construction as the high pressure generator; the ammonia vapor goes to the rectifier where it is purified. The balances are as follows:

$$\dot{Q}_{REC2} = \dot{m}_{14a}h_{14a} - \dot{m}_{14b}h_{14b} - \dot{m}_{14}h_{14} \tag{2.14}$$

$$\dot{Q}_{HPC} = \dot{m}_{11}h_{11} - \dot{m}_{12}h_{12} \tag{2.15}$$

$$\dot{Q}_{IPG} = \dot{m}_{15}h_{15} + \dot{m}_{14a}h_{14a} - \dot{m}_{10}h_{10} - \dot{m}_{14b}h_{14b} \tag{2.16}$$

Where the following energy balance should hold:

$$\dot{m}_{10}h_{10} + \dot{m}_{11}h_{11} + \dot{m}_{14b}h_{14b} = \dot{m}_{15}h_{15} + \dot{m}_{12}h_{12} + \dot{m}_{14a}h_{14a} \tag{2.17}$$

Or:

$$\dot{Q}_{HPC} = \dot{Q}_{IPG} \tag{2.18}$$

For the second rectifier the mass balances are as follows:

$$\dot{m}_{14a} = \dot{m}_{14b} + \dot{m}_{14} \tag{2.19}$$

$$y_{14a}\dot{m}_{14a} = x_{14b}\dot{m}_{14b} + y_{14}\dot{m}_{14} \tag{2.20}$$

Furthermore, the following assumptions apply:

$$T_{14} = T_1 + 30K \tag{2.21}$$

$$T_{14b} = T_{14} - 20K \tag{2.22}$$

The reflux ratio can be calculated with:

$$RR_{REC2} = \frac{m_{14b}}{m_{14}} = \frac{y_{14a} - y_{14}}{x_{14b} - y_{14a}} \tag{2.23}$$

To determine the temperature at the solution outlet of the intermediate pressure generator a pinch temperature is assumed. This gives us the following relation:

$$T_{15} = T_{12} + 5K \tag{2.24}$$

Condenser In the condenser heat is exchanged and a saturated liquid leaves the condenser. The balances for the condenser are:

$$\dot{m}_{14} + \dot{m}_{13} = \dot{m}_1 \tag{2.25}$$

$$y_{14}\dot{m}_{14} + y_{13}\dot{m}_{13} = x_1\dot{m}_1 \tag{2.26}$$

$$\dot{Q}_{CON} = \dot{m}_{14}h_{14} + \dot{m}_{13}h_{13} - \dot{m}_1 h_1 \tag{2.27}$$

Absorber In the absorber, the solution coming from the intermediate pressure generator (stream 17) absorbs the vapor coming from the evaporator (stream 3). The rich solution leaves the absorber (stream 4) and gets pumped to the high pressure generator. During this process the absorber exchanges heat with the environment ($\dot{Q}_{ABS}$). The balances for the absorber are:

$$\dot{m}_3 + \dot{m}_{17} = \dot{m}_4 \tag{2.28}$$

$$y_3\dot{m}_3 + x_{17}\dot{m}_{17} = x_4\dot{m}_4 \tag{2.29}$$

$$\dot{Q}_{ABS} = \dot{m}_3 h_3 + \dot{m}_{17}h_{17} - \dot{m}_4 h_4 \tag{2.30}$$

Evaporator The evaporator exchanges heat with the environment ($\dot{Q}_{EVA}$) while evaporating the ammonia flow. The ammonia leaves the evaporator as a saturated vapor (stream 3). The balances for the evaporator are:

$$\dot{m}_2 = \dot{m}_3 \tag{2.31}$$

$$x_2\dot{m}_2 = x_2\dot{m}_3 \tag{2.32}$$

$$\dot{Q}_{EVA} = \dot{m}_3 h_3 - \dot{m}_2 h_2 \tag{2.33}$$

Heat exchangers (HEX1 and HEX2) To reduce the required heat input, two solution heat exchangers are used. Both heat exchangers are modelled using a pinch temperature of 5 K. The solution flows and their temperatures are illustrated in figure 2.6 and 2.7. Heat exchanger 1 uses the following balances:

$$\dot{m}_6(h_7 - h_6) = \dot{m}_8(h_8 - h_9) \tag{2.34}$$

$$T_9 = T_6 + 5K \tag{2.35}$$

The balance and assumption for heat exchanger 2 are as follows:

$$\dot{m}_5(h_6 - h_5) = \dot{m}_{15}(h_{15} - h_{16}) \tag{2.36}$$

$$T_{16} = T_5 + 5K \tag{2.37}$$

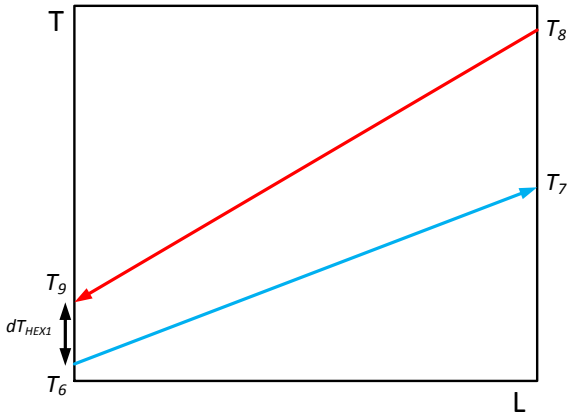

Figure 2.6: Illustration the pinch temperature in the first heat exchanger. The temperature profile of the hot stream is shown in red and the cold stream in blue. The pinch temperature is assumed to be 5 K.

.

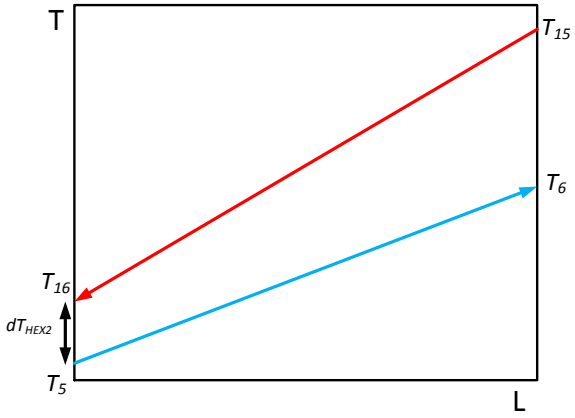

Figure 2.7: Illustration the pinch temperature in the second heat exchanger. The temperature profile of the hot stream is shown in red and the cold stream in blue. The pinch temperature is assumed to be 5 K.

.

Valves All the valves are modelled isenthalpic which gives the following balances:

$$h_{16} = h_{17} \tag{2.38}$$

$$h_9 = h_{10} \tag{2.39}$$

$$h_{12} = h_{13} \tag{2.40}$$

$$h_1 = h_2 \tag{2.41}$$

Now that $\dot{Q}_{EVA}$, $\dot{Q}_{CON}$, $\dot{Q}_{ABS}$ and $\dot{Q}_{HPG}$ are calculated, $COP_{heating}$ and $COP_{cooling}$ can be calculated using equation 2.1 and 2.2. The main calculation procedure is illustrated in figure 2.8. It makes use of three iterative loops. Firstly, the minimum concentration of the refrigerant flows is assumed (y_{11} and y_{14}). For some operating conditions and design parameters, the vapor leaving one of the rectifiers can have a higher temperature than the vapor entering the rectifier which results in a negative reflux flow. In order to prevent this, the minimum purity of the refrigerant flows will be increased. For the last iteration loop T_{12} will be increased until equation 2.17 is satisfied. All the equations and iterative loops are implemented in the software package MATLAB [20].

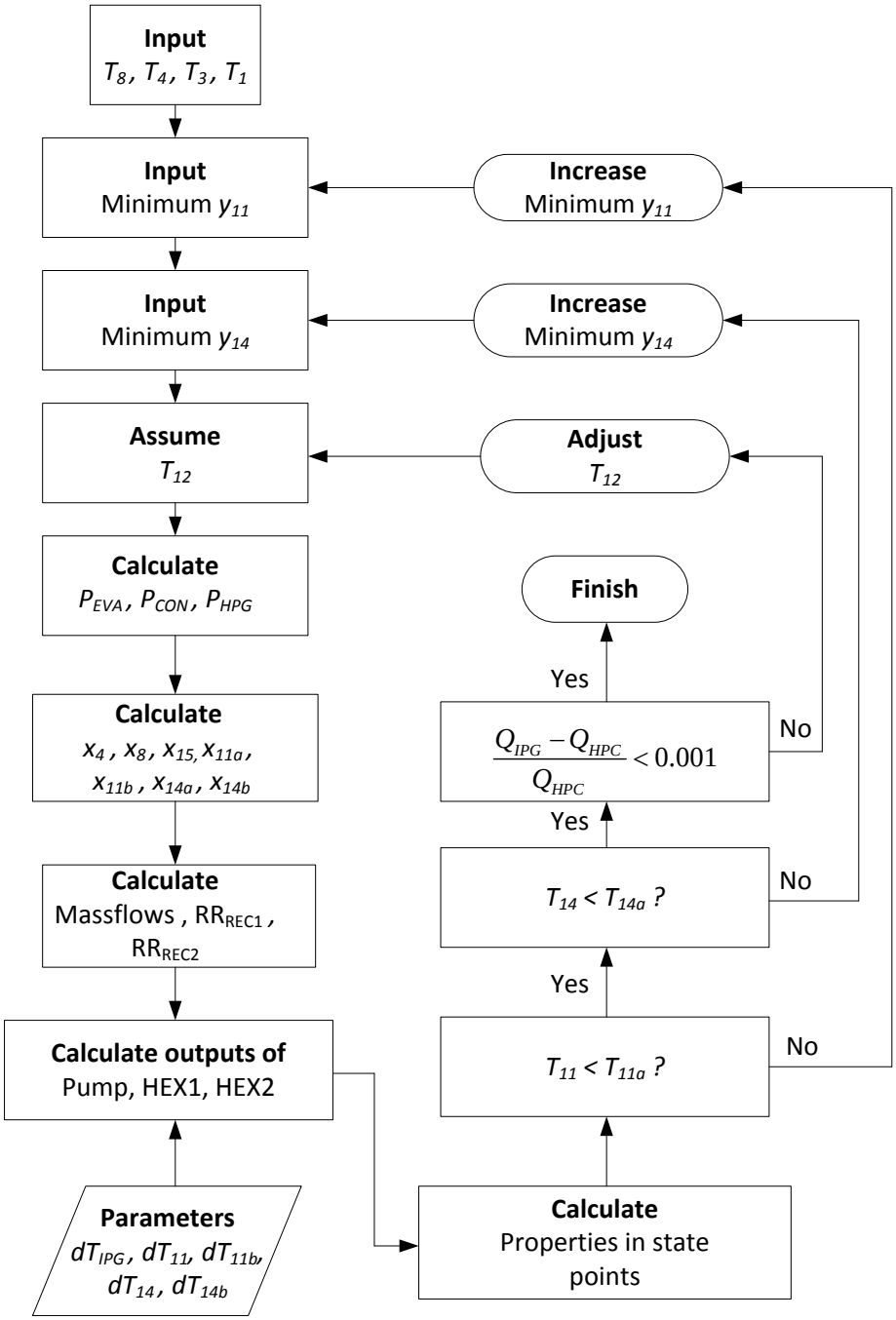

Figure 2.8: Main calculation procedure for the double-effect absorption system in a series configuration. There are three iteration loops. Once the balance between the high pressure condenser and the intermediate pressure generator is satisfied the loop finishes.

2.3. Results and discussion

2.3.1. Cycle performance

This section discusses the behaviour and performance of the developed thermodynamic model. The operating conditions and design parameters are listed in table 2.1. These conditions have a strong impact on the performance. For the discussed case, the cycle uses waste heat at a temperature of 130 °C and it will supply the cooling demand at 0 °C. The absorber, the condenser and the rectifiers exchange heat with the environment at a temperature of 30 °C. The load of each component and the coefficient of performance of the absorption cycle under these conditions are shown in table 2.2. The performance of this cycle under these conditions is lower than the lithium-bromide and water double effect absorption system. However, this cycle does perform better than the single-effect absorption cycle using ammonia-water. All the properties at the state points are listed in table 2.3. As can be seen in table 2.2, the required pump power has a small effect on the performance.

Table 2.1: Operating conditions and design parameters for the double-effect absorption cycle during cooling. All input parameters for the mathematical model. Their influence on the performance of the cycle is investigated in chapter 2.3.3

Symbol	Value	Unit	Description
T_{CON}	30	[°C]	Condensation temperature
T_{ABS}	30	[°C]	Temperature of the absorber solution outlet
T_{HPG}	130	[°C]	High pressure generator solution outlet temperature
T_{EVA}	0	[°C]	Evaporation temperature
dT_{IPG}	5	[K]	Pinch temperature in the intermediate pressure generator
dT_{HEX1}	5	[K]	Pinch temperature in the first heat exchanger
dT_{HEX2}	5	[K]	Pinch temperature in the second heat exchanger
η_{PUMP}	0.9	[-]	Pump efficiency
y_{NH3}	0.999	[-]	Purity of ammonia in the refrigerant cycle
$\dot{m}_5$	1	[kg/s]	Mass flow through the pump
dT_{11}	30	[K]	Temperature difference between T_{11} and T_{12}
dT_{11b}	10	[K]	Temperature difference between T_{11b} and T_{12}
dT_{14}	30	[K]	Temperature difference between T_{14} and T_1
dT_{14b}	10	[K]	Temperature difference between T_{14b} and T_1

Table 2.2: Results obtained from the model. The results for the mathematical model for the conditions: T_{ABS} = T_{CON} = 30 °C, T_{EVA} = 0 °C and T_{HPG} = 130 °C. All other the input values for these results are listed in table 2.1.

Symbol	Value	Unit	Description
$\dot{Q}_{EVA}$	102.39	[kW]	Heat flow in the evaporator
$\dot{Q}_{ABS}$	146.84	[kW]	Heat flow in the absorber
$\dot{Q}_{COND}$	52.136	[kW]	Heat flow in the condenser
$\dot{Q}_{HPG}$	118.63	[kW]	Heat added to the High pressure generator
$\dot{Q}_{IPG}$	56.730	[kW]	Heat exchanged in the intermediate pressure generator
W_{PUMP}	4.6977	[kW]	Pump power
$\dot{Q}_{REC1}$	23.032	[kW]	Heat rejected in the first rectifier
$\dot{Q}_{REC2}$	3.2856	[kW]	Heat rejected in the second rectifier
$COP_{cooling}$	0.83022	[-]	COP for cooling
RR_{REC1}	0.3002	[-]	Reflux ratio in the first rectifier
RR_{REC2}	0.0505	[-]	Reflux ratio in the second rectifier

2.3.2. Influence of the operating conditions on the performance

In order to find the most suitable application for this absorption cycle using ammonia and water, it is useful to look at the influence of the operating condition on the performance. Figure 2.9 shows the COP for different evaporator outlet temperatures while varying the outlet temperature of the high pressure generator. There is a minimum T_{HPG} for every evaporator temperature. To explain this minimum, we have to take a closer look at the high pressure generator. At point 7 we have the strong solution at the inlet of the high pressure generator from which ammonia will be desorbed. The concentration of stream 7 is the same as the stream leaving the absorber (stream 4) which is determined by P_{EVA} and T_{ABS}. By increasing T_{EVA}, the evaporator pressure P_{EVA} also increases. The ammonia concentration of the solution increases with increasing pressure so the concentration of the high pressure generator inlet becomes higher with increasing evaporator outlet temperature. When the concentration of the high pressure generator inlet is higher, more ammonia can be evaporated which explains the higher COP for higher evaporator temperatures. Of course the concentration of the solution leaving the high pressure generator has to be lower than the concentration of the inlet. So if T_{HPG} becomes too low, the concentration of the outlet will become higher than the concentration of the inlet causing the system to fail which explains the minimum T_{HPG}. For lower evaporation temperatures it is beneficial to have higher T_{HPG} because this results in a higher COP. Because this model assumes equilibrium conditions at stream 11a, the temperature at this point cannot be higher than the critical temperature which is dependent on the composition of the solution. When increasing T_{HPG}, the ammonia concentration of stream 11a decreases so the critical temperature increases. Unfortunately, the temperature of the stream increases faster than the critical temperature with increasing T_{HPG} so a maximum will be reached.

Figure 2.10 shows the COP of the absorption cycle for different absorber and condenser outlet temperatures. The performance of the cycle is significantly lower for higher absorber and condenser outlet temperatures. Additionally, the operating range is a lot smaller for higher absorber and condenser outlet temperatures. When the condenser outlet temperature increases, the intermediate pressure P_{CON} also increases. This increases the lowest solution concentration level (x_{15}) which has to be lower than the absorber outlet concentration (x_4). In turn, when increasing T_{HPG} the lowest solution concentration level goes up. This means that for higher absorber and condenser outlet temperatures there is a higher minimum T_{HPG}.

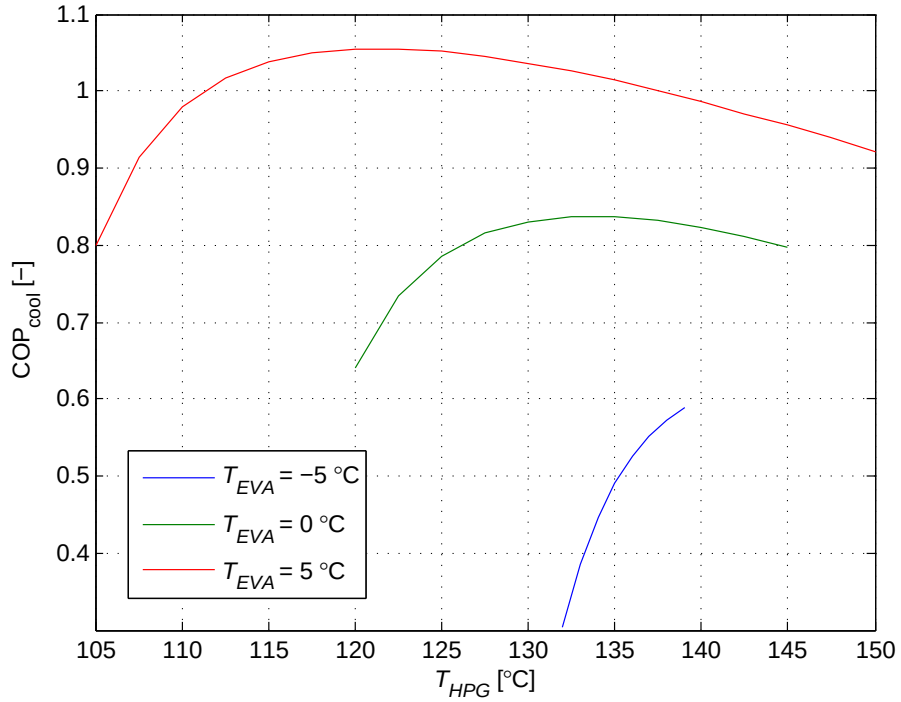

Figure 2.9: The COP of the double effect absorption cycle as a function of the outlet solution temperature of the high pressure generator for different evaporator temperatures. The COP is displayed for different evaporation temperatures. The absorber and condenser temperature are kept constant at 30 °C, all other parameters are listed in table 2.1

.

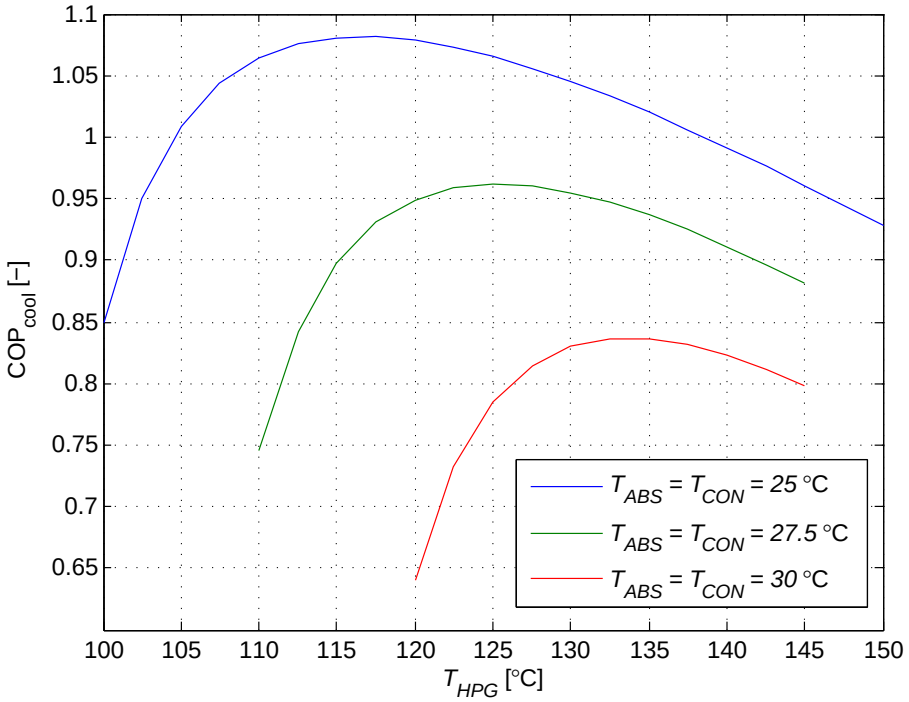

Figure 2.10: The COP of the double effect absorption cycle as a function of the outlet solution temperature of the high pressure generator for different absorber and condenser temperatures. The COP is displayed for different absorber and condenser temperatures. The evaporation temperature is kept constant at 0 °C, all other parameters are listed in table 2.1

Table 2.3: State properties of the double effect absorption cycle during cooling. for the conditions: T_{ABS} = T_{CON} = 30 °C, T_{EVA} = 0 °C and T_{HPG} = 130 °C. All other operating parameters are listed in table 2.1 . The heat flows and reflux ratios are displayed in table 2.2.

	Massflow [kg/s]	**Temperature [°C]**	**Concentration**	**Pressure [bar]**	**Enthalpy [kJ/kg]**
1	0.087	30.000	0.999	11.670	485.202
2	0.087	0.031	0.999	4.294	485.202
3	0.087	0.000	0.999	4.294	1660.177
4	1.000	30.000	0.510	4.294	47.630
5	1.000	30.305	0.510	39.471	51.857
6	1.000	64.320	0.510	39.471	223.835
7	1.000	121.519	0.510	39.471	516.406
8	0.944	130.000	0.481	39.471	544.827
9	0.944	69.320	0.481	39.471	234.892
10	0.944	69.678	0.481	11.670	234.892
11	0.056	107.792	0.999	39.471	1743.889
11a	0.073	121.519	0.966	39.471	1803.238
11b	0.017	87.792	0.858	39.471	631.678
12	0.056	77.791	0.999	39.471	731.337
13	0.056	30.047	0.999	11.670	731.337
14	0.031	60.000	0.999	11.670	1717.515
14a	0.033	69.678	0.989	11.670	1750.151
14b	0.002	40.000	0.785	11.670	311.560
15	0.913	72.792	0.463	11.670	242.946
16	0.913	35.305	0.463	11.670	54.551
17	0.913	35.413	0.463	4.294	54.551

Figure 2.11 shows the reflux ratio for the high pressure generator at different T_{HPG}. When T_{HPG} increases, the inlet temperature (stream 7) of the high pressure generator also increases because they exchange heat in HEX1. Stream 7 and stream 11a are assumed to be in equilibrium, so T_{11a} increases with increasing T_{HPG} giving the stream a lower concentration. When stream 11a has a lower concentration, more water has to be removed from this stream in the rectifier, resulting in a higher reflux ratio.

Figure 2.12 shows the heat flow in the high pressure generator and the evaporator with varying T_{HPG}. With increasing T_{HPG} both heat flows increase, however, the high pressure generator input heat increases with a higher rate. This means that there is an optimum COP and it will decrease for higher temperatures. When the temperature increases, there is more water content in the vapor leaving the high pressure generator. This extra water content does not contribute to the cooling power, but it does need more heat input to evaporate.

Figure 2.13 shows the amount of heat that has to be extracted in the rectifiers to condens the water content in the vapor. The rejected heat in the first rectifier is strongly dependent on the high pressure generator solution outlet temperature. This explains why the high pressure generator input heat increases faster than the cooling power, and thus why the COP decreases with increasing T_{HPG}.

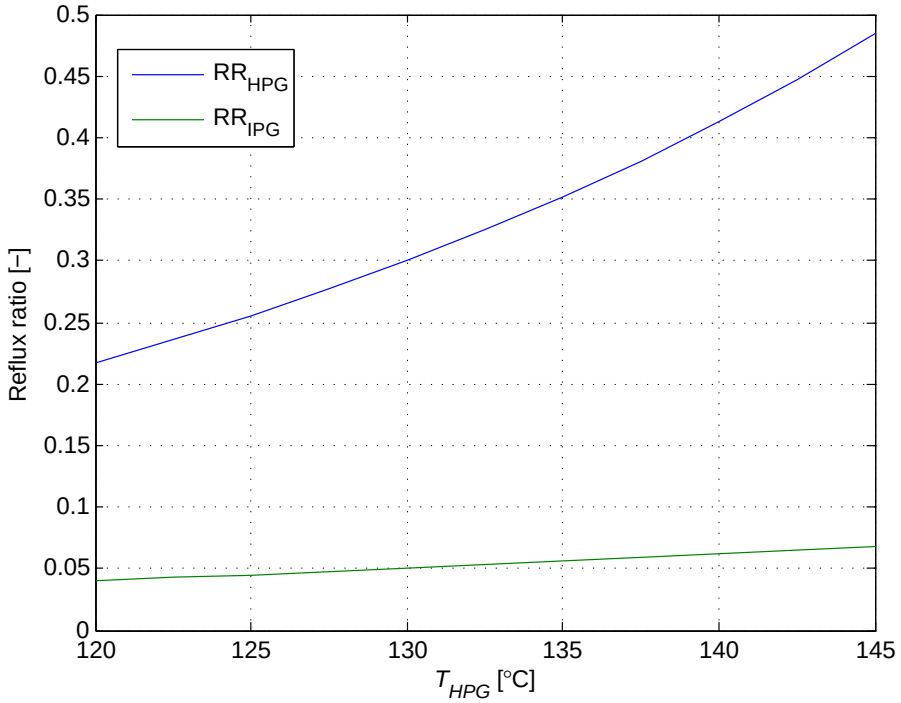

Figure 2.11: The reflux ratio of the rectifier of the high pressure generator for different absorber and condenser properties. For the conditions: T_{ABS} = T_{CON} = 30 °C and T_{EVA} = 0 °C. The reflux ratio is calculated with equation 2.13. The high pressure generator reflux ratio shows a stronger increase because it is directly connected to the high pressure generator

.

2.3.3. Influence of the design parameters on the performance

Figure 2.14 shows the COP as a function of the ammonia purity in the refrigerant stream. From the figure it can be seen that the COP decreases with increasing purity. This is because more heat has to be removed from the stream to condens the water. This heat has to be added in the high pressure generator resulting in a lower COP.

Figure 2.15 shows the COP of the cycle as a function of the superheating temperature of the vapor stream leaving the rectifiers. This is the temperature difference between T_{12} and T_{11} and T_1 and T_{14}. In this model, a superheating temperature of 30 K is assumed. Increasing the superheating temperature of stream 11 results in a higher COP for cooling applications. When the superheating temperature increases, more heat is rejected in the high pressure condenser and released to the intermediate pressure generator, which in turn, has more heat to generate more ammonia. However, increasing the superheating temperature in the second rectifier (dT_{14}) has no effect on the COP for a cooling application. A higher superheating temperature does result in a higher enthalpy at point 14, but this extra energy is rejected to the environment in the second rectifier and the condenser, which does not have an effect on the COP.

Figure 2.16 shows the temperature difference between the temperature of the superheated vapor and the temperature of the liquid reflux stream leaving the rectifiers. The COP for a cooling application increases when increasing dT_{14b} and dT_{11b}.

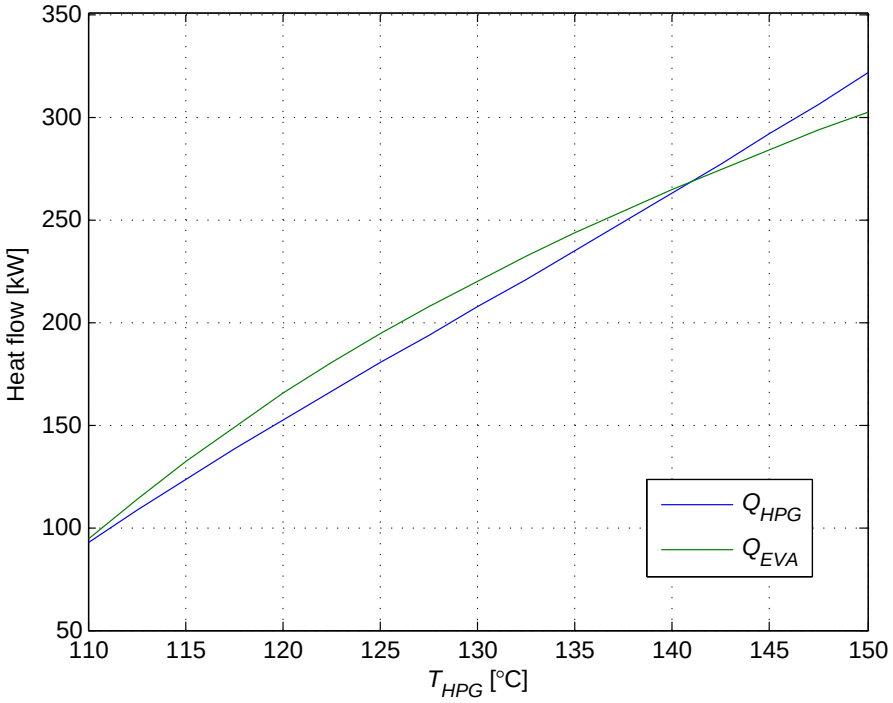

Figure 2.12: The heat flow in the high pressure generator and the evaporator. For the operating conditions: T_{ABS} = T_{CON} = 30 °C and T_{EVA} = 0 °C. The high pressure generator heat flows shows a stronger increase resulting in a lower COP for higher T_{HPG}.

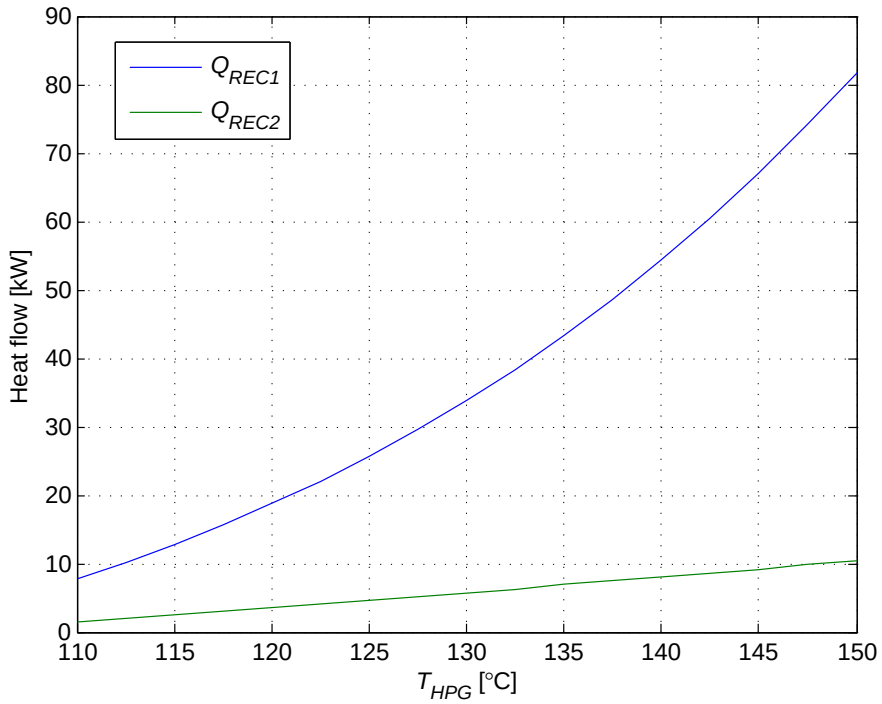

Figure 2.13: The heat flow in the rectifiers. For the operating conditions: T_{ABS} = T_{CON} = 30 °C and T_{EVA} = 0 °C. The first rectifier shows a much stronger increase because it is directly connected to the high pressure generator. When the high pressure generator operates at higher temperatures, more water has to be condensed from the vapor stream.

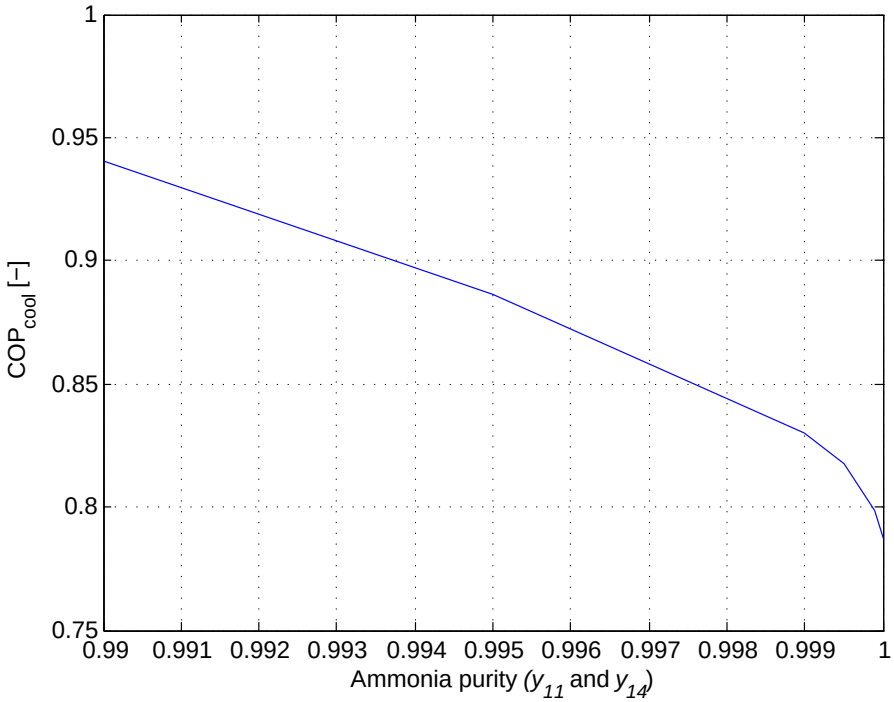

Figure 2.14: The COP of the double effect absorption cycle as a function of the ammonia purity in the refrigerant stream. For the conditions: T_{ABS} = T_{CON} = 30 °C, T_{EVA} = 0 °C and T_{HPG} = 130 °C. All other operating conditions and design parameters are listed in table 2.1. A strong decrease in COP for higher purities can be seen because more heat is rejected to the environment in the rectifiers.

2.4. Conclusions

In this chapter, the mathematical modelling of the double-effect ammonia water absorption cycle has been described in detail. The purpose of the model is to investigate the suitability of the ammonia water working pair in this cycle for cooling or heating applications. Additionally, the model can be used to investigate the effect of different operating conditions and design parameters on the performance. The mass and energy balances of all the individual components are implemented and solved using the software package Matlab, where the properties of the ammonia and water mixture are taken from NIST's REFPROP database. Based on the findings of this model, the following conclusions are drawn:

- For temperatures above 0 °C, lithium bromide as working pair for this cycle has the preference because the performance is significantly better.
- The necessity of rectification has a negative effect on the performance.
- For high absorber and condenser outlet temperatures the cycle has a very small operating range so the cycle is not suitable for heating applications.
- The pump power has a small effect on the performance of the cycle.

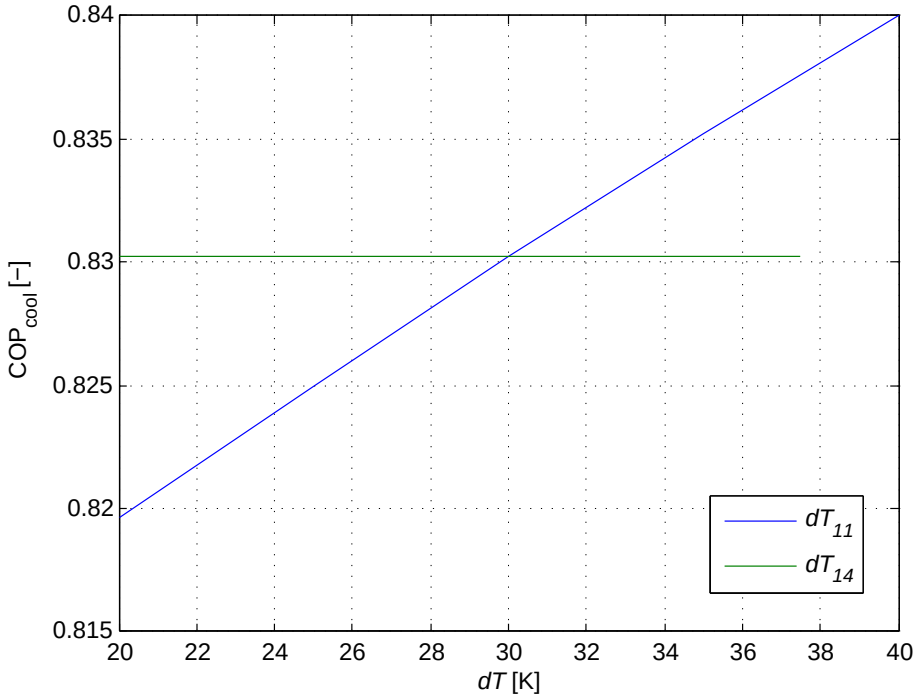

Figure 2.15: The COP of the double effect absorption cycle as a function of the superheating temperature of the vapor leaving the high pressure generator. For the conditions T_{ABS} = T_{CON} = 30 °C, T_{EVA} =0 °C and T_{HPG} = 130 °C. All other operating conditions and design parameters are listed in table 2.1.

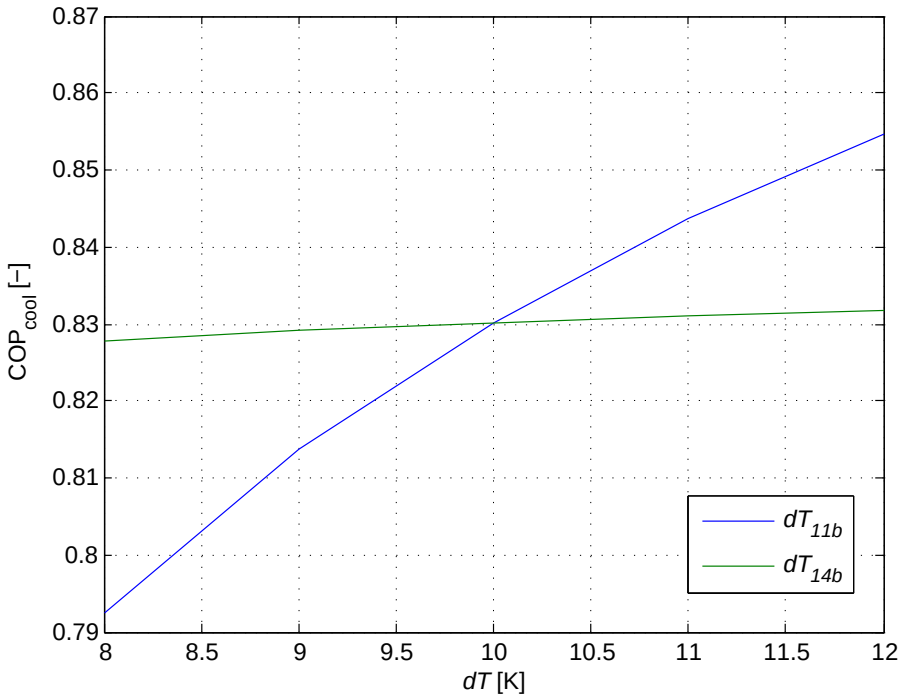

Figure 2.16: The COP of the double effect absorption cycle as a function of the temperature difference of the liquid reflux streams leaving the rectifiers. For the conditions T_{ABS} = T_{CON} = 30 °C, T_{EVA} =0 °C and T_{HPG} = 130 °C. All other operating conditions and design parameters are listed in table 2.1.

3

Double-effect absorption cycle with ammonia-ionic liquid working pairs

3.1. Introduction

This chapter describes a method to determine vapor-liquid equilibrium and enthalpy properties for nine ionic liquid and ammonia working pairs from experimental data. The properties are used to predict the performance of the nine working pairs in a double-effect absorption cycle. A method to predict the suitability of the working pairs without doing any cycle calculations is presented and the influence of the design parameters and the operating conditions on the performance is discussed.

3.2. Properties

Vapor-liquid equilibrium and enthalpy are two of the fundamental properties to calculate the performance of working pairs for absorption cycles. They describe the relationship between the pressure, temperature and composition and those with the enthalpy respectively. Equations 3.1-3.6 describe a non-random two-liquid (NRTL) model to predict the vapor liquid equilibrium of mixtures. Due to the non-volatility of ionic liquids, its fraction in the vapor phase can be neglected. In that case, the equilibrium criterion can be simplified to equation 3.1 where $P^{sat}_{NH_3}$ can be obtained from NIST's Refprop [17]. With experimental vapor liquid equilibrium data the binary parameters α,$\tau^{(0)}_{12}$, $\tau^{(1)}_{12}$, $\tau^{(0)}_{21}$ and $\tau^{(1)}_{21}$ in the NRTL model are correlated and will allow for the determination of the operating concentrations. The correlated parameters are listed in table 3.1. Eight of the nine working pairs have been correlated with a Root-mean-square deviation (RMSD) smaller than 5.6 %. Only the model for the working pair ammonia and [Omim][BF4] showed a slightly larger deviation of 8.7 %. The equations are implemented in the software package Matlab by Wang and Ferreira [33].

$$\gamma_{NH_3} = \frac{P}{x_{NH_3} P^{sat}_{NH_3}} \tag{3.1}$$

The activity coefficient γ_{NH_3} needed for equation 3.1 can be obtained by the NRTL activity coefficient model:

$$\ln(\gamma_i) = x_2^2 \left[\tau_{21} \left(\frac{G_{21}}{x_1 + x_2 G_{21}} \right)^2 + \frac{G_{12}\tau_{12}}{(x_2 + x_1 G_{12})^2} \right] \tag{3.2}$$

Where the NRTL parameters can be calculated with equation 3.3-3.6.

$$G_{12} = \exp(-\alpha\tau_{12}) \tag{3.3}$$

$$G_{21} = \exp(-\alpha\tau_{21}) \tag{3.4}$$

$$\tau_{12} = \tau_{12}^{(0)} + \frac{\tau_{12}^{(1)}}{T} \tag{3.5}$$

$$\tau_{21} = \tau_{21}^{(0)} + \frac{\tau_{21}^{(1)}}{T} \tag{3.6}$$

The enthalpy data for pure ammonia is directly obtained from NIST's REFPROP [17]. For a real solution the total enthalpy can be calculated as the sum of the enthalpy for the ideal solution and the mixing heat, which is expressed by equation 3.7.

$$h = x_{NH_3} h_{NH_3} + x_{IL} h_{IL} + h_{mix} \tag{3.7}$$

In this work, the mixing heat part h_{mix}, is neglected. This means that the equation simplifies to:

$$h = x_{NH_3} h_{NH_3} + x_{IL} h_{IL} \tag{3.8}$$

The enthalpy of the pure ionic liquid can be obtained from the heat capacity of the pure ionic liquid according to equation 3.9.

$$h_{IL} = h_0 + \int_{T_0}^{T} c_p^{IL} dT \tag{3.9}$$

Where the heat capacity can be expressed by the linear equation 3.10, using the correlated parameters listed in table 3.2. Furthermore, to prevent the ionic liquids from chemically decomposing, the cycle should operate below the decomposition temperatures. For eight of the nine ionic liquids the decomposition is known from experimental data, they are listed in table 3.3. The ionic liquid [Emim][SCN] has the lowest decomposition temperature of 250 °C, which is below conventional operating temperatures of the double-effect absorption cycle.

$$c_p = c_0 + c_1 T \tag{3.10}$$

Table 3.1: Correlated binary parameters in the NRTL model. The NRTL parameters are correlated using experimental data of vapor-liquid equilibrium measurements. The maximum RMSD is 8.71% [33].

Absorbent	α	$\tau_{12}^{(0)}$	$\tau_{12}^{(1)}$	$\tau_{21}^{(0)}$	$\tau_{21}^{(1)}$	**Data source**
[Bmim][BF4]	-0.01296	-48.0115	8926.476	32.42976	-5461.79	Yokozeki and Shiflett [37]
[Bmim][PF6]	0.334114	3.729984	-509.569	-4.18755	643.4984	Yokozeki and Shiflett [37]
[Emim][BF4]	0.999524	-0.00571	236.4087	-1.25914	164.5906	Li et al. [18]
[Emim][EtOSO3]	0.716041	11.16699	-4089.25	-7.52981	2451.455	Yokozeki and Shiflett [36]
[Emim][SCN]	-0.27082	-10.6616	3120.011	5.600432	-1967.71	Yokozeki and Shiflett [36]
[Emim][Tf2N]	-0.00422	-99.9992	14710.17	71.51013	-9046.21	Yokozeki and Shiflett [37]
[Hmim][BF4]	0.999976	-14.8044	5081.738	-2.66902	478.851	Li et al. [18]
[Mmim][DMP]	0.240323	7.819133	-2300.68	-4.42766	1000.393	Sun et al. [31]
[Omim][BF4]	0.907017	-7.01386	2690.743	-2.39948	283.1702	Li et al. [18]

Table 3.2: Correlated parameters. In the equation $c_p = c_0 + c_1 T$ for mole-based c_p. The maximum RMSD is 0.94% [33]

Absorbent	c_0	c_1	**Data source**
[Bmim][BF4]	250.2006	0.39721	Paulechka et al. [25]
[Bmim][PF6]	282.0703	0.452468	Kabo et al. [14]
[Emim][BF4]	214.0669	0.307615	Yu et al. [38]
[Emim][EtOSO3]	245.5262	0.461986	Paulechka et al. [25]
[Emim][SCN]	116.4736	0.546945	Navarro et al. [21]
[Emim][Tf2N]	363.1883	0.478096	Paulechka et al. [24]
[Hmim][BF4]	275.962	0.52	Waliszewski [32]
[Mmim][DMP]	-153.898	1.476179	He et al. [12]
[Omim][BF4]	323.8942	0.587683	Paulechka et al. [25]

Table 3.3: Decomposition temperatures. The temperature at which the ionic liquids start to chemically decompose, the operating temperature range of the investigated absorption cycle is below this limit.

Absorbent	T_{dec} [°C]	**Reference**
[Bmim][BF4]	>407	Fang et al. [11]
[Bmim][PF6]	>329	Cao and Mu [5]
[Emim][BF4]	>333	Cao and Mu [5]
[Emim][EtOSO3]	>330	Wasserscheid and Welton [34]
[Emim][SCN]	>250	Navarro et al. [21]
[Emim][Tf2N]	>330	Chen et al. [7]
[Hmim][BF4]	>332	Cao and Mu [5]
[Omim][BF4]	>313	Cao and Mu [5]

3.3. Thermodynamic model

A simplified process flow diagram of the double effect absorption cycle in series configuration is shown in figure 3.1. This model is similar to the model for the ammonia water working pair from chapter 2. However, as the ionic liquids are assumed to be non-volatile, there is no need for rectifiers. Without rectifiers, the energy balances for the high pressure generator, the absorber, the condenser, the evaporator and the intermediate pressure generator are given by equation 3.11-3.15. Furthermore, the refrigerant flow is modeled as pure ammonia and the design parameters are listed in table 3.4. The main calculation procedure is illustrated in figure 3.2.

$$\dot{Q}_{HPG} = \dot{m}_8 h_8 + \dot{m}_{11} h_{11} - \dot{m}_7 h_7 \tag{3.11}$$

$$\dot{Q}_{ABS} = \dot{m}_{17} h_{17} + \dot{m}_3 h_3 - \dot{m}_4 h_4 \tag{3.12}$$

$$\dot{Q}_{CON} = \dot{m}_{14} h_{14} + \dot{m}_{13} h_{13} - \dot{m}_1 h_1 \tag{3.13}$$

$$\dot{Q}_{EVA} = \dot{m}_3 h_3 - \dot{m}_2 h_2 \tag{3.14}$$

$$\dot{m}_{11}(h_{11} - h_{12}) = \dot{m}_{14} h_{14} + \dot{m}_{15} h_{15} - \dot{m}_{10} h_{10} \tag{3.15}$$

To quantify the performance of the model, equations 3.16 and 3.17 are used to calculate the COP for cooling and heating applications respectively.

$$COP_{cooling} = \frac{\dot{Q}_{EVA}}{\dot{Q}_{HPG}} \tag{3.16}$$

$$COP_{heating} = \frac{\dot{Q}_{ABS} + \dot{Q}_{CON}}{\dot{Q}_{HPG}} \tag{3.17}$$

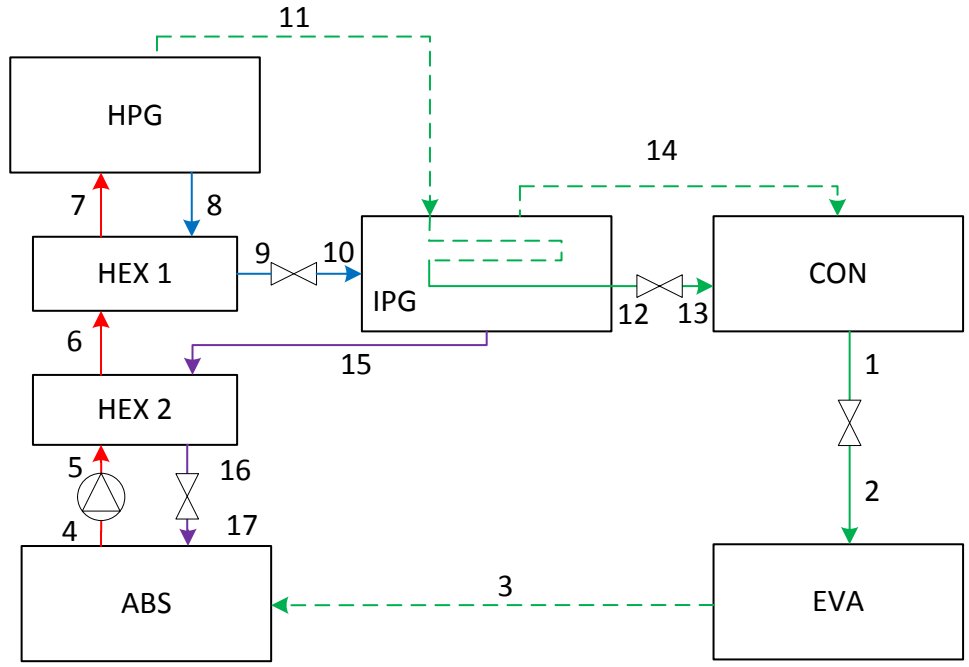

Figure 3.1: Process flow diagram of the double-effect absorption cycle in a series configuration. The red, blue, purple and green lines indicate the strong solution, the intermediate solution, the weak solution and the refrigerant flows, respectively. The dotted lines indicate the vapor phase and the solid lines indicate the liquid phase.

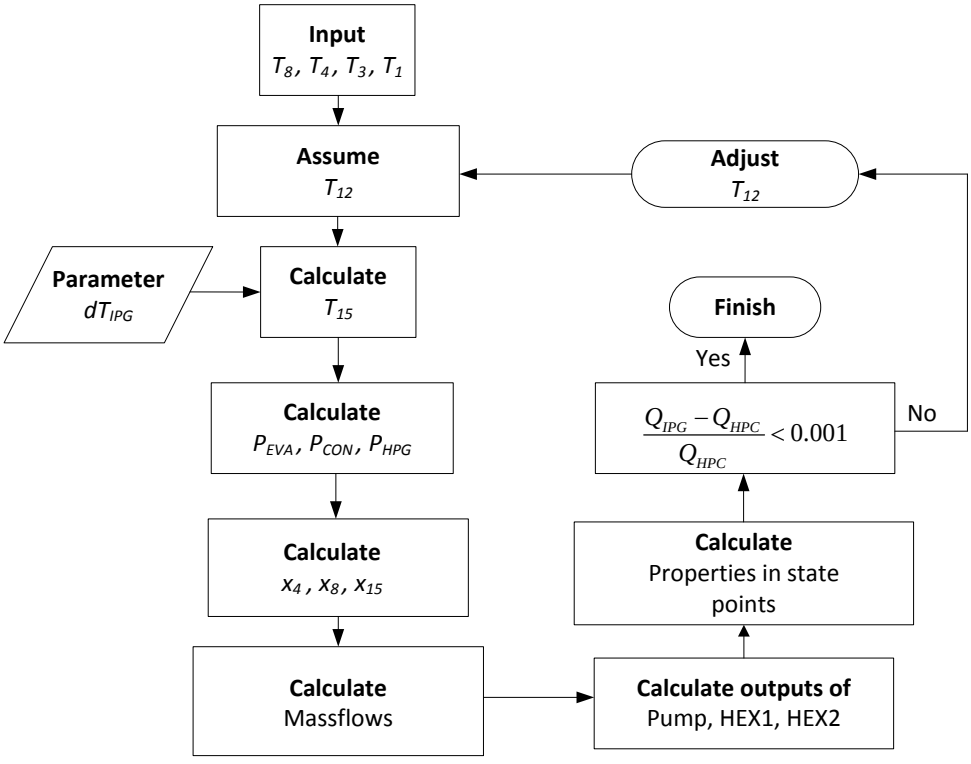

Figure 3.2: Main calculation procedure for the double-effect absorption system in a series configuration without rectifiers. In contrast to the calculation procedure using ammonia and water as working pair, there is only one iteration loop because there are no rectifiers in the cycle.

Table 3.4: Design parameters for the double-effect absorption cycle using ammonia and ionic liquids as working pair. The mass flow through the pump can be adjusted to increase all the heat flows, and thus the heating or cooling demand. The influence of the design parameters is discussed later.

Symbol	Value	Unit	description
dT_{IPG}	5	[K]	Pinch temperature in the IPG
dT_{HEX1}	5	[K]	Pinch temperature in HEX1
dT_{HEX2}	5	[K]	Pinch temperature in HEX2
η_{PUMP}	0.9	[-]	Pump efficiency
$\dot{m}_4$	1	[kg/s]	Mass flow through the pump

3.4. Results and discussion

3.4.1. Thermodynamic restrictions

The range of working conditions for the working pairs can be determined without making any absorption cycle calculations. By using vapor liquid equilibrium data and restrictions of the thermodynamic model, the limits of the operating conditions can be determined. In the intermediate pressure generator and the high pressure generator, the concentration of the solution at the outlets (stream 8 and 15) should be smaller than at the inlets (stream 7 and stream 10). For the absorber the solution outlet concentration should be higher. So the restrictions for the absorber, high pressure generator and intermediate pressure generator are respectively:

$$x_4 > x_{17} \tag{3.18}$$

$$(x_7 = x_4) > x_8 \tag{3.19}$$

$$x_{10} > (x_{15} = x_{17}) \tag{3.20}$$

As explained in chapter 2, the thermodynamic model finds a T_{12} for which the energy is balanced in the cycle, when equation 3.15 is satisfied. By using the restrictions and VLE-data, the range of T_{12} can be determined. Every restriction gives a limit for T_{12}. To determine these limits, we take a closer look at the phase diagrams (figure 3.3- 3.5). The outlet of the evaporator is pure saturated ammonia vapor at a temperature T_{EVA}. This gives us the lowest pressure level P_{EVA}. From P_{EVA} and T_{ABS} the strongest solution concentration x_4 can be determined. The intermediate pressure level P_{CON} is determined by T_{CON}. This means that the only parameters that are fixed by the operating conditions are P_{EVA}, P_{CON} and x_4. All other parameters are directly or indirectly dependent on T_{12}.

Restriction from the absorber The absorber operates at P_{EVA}, and the strong solution outlet has a temperature T_{ABS} giving us the strong solution outlet concentration x_4, the blue line in figure 3.3. The concentration of the absorber solution inlet (stream 17) is determined at the outlet of the intermediate pressure generator (stream 15) which operates at P_{CON} and T_{15}. The limit where the absorber can operate is at x_4=x_{17}. To determine the corresponding minimum temperature of this limit we have to solve:

$$x_4(T_{ABS}, P_{EVA}) = x_{15}(T_{15}, P_{CON}) \tag{3.21}$$

By using the pinch temperature of the intermediate pressure generator (T_{12}=T_{15}+5K), a minimum temperature of T_{12}, shown in figure 3.3, can be found. When T_{12} becomes lower than this value, x_{15} becomes higher than x_4 causing the absorber to fail.

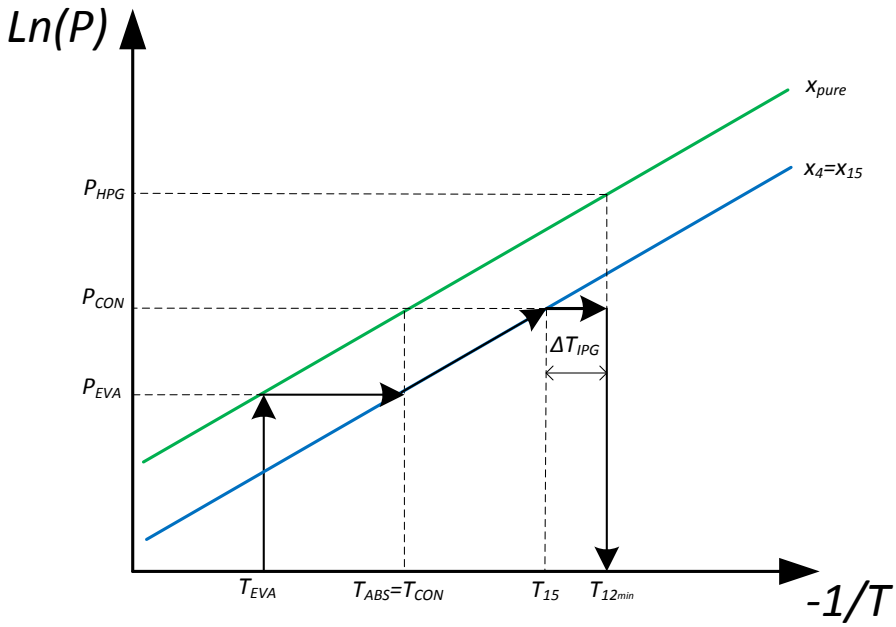

Figure 3.3: ln(P) - 1/T phase diagram to find a minimum temperature for T12. Resulting from the restriction of the absorber. The green and blue line indicate the pure ammonia line and the solution concentration line, respectively. Horizontal lines are isobars, vertical lines are isotherms and isoconcentration lines are diagonal.

Restriction from the high pressure generator To determine the upper limit of T_{12} we take a look at the high pressure generator and equation 3.19. The limit where the high pressure generator can operate is at x_4=x_8 (wherex_4=x_7). To find this limit we have to find a solution for equation 3.22.

$$x_4(T_{ABS}, P_{EVA}) = x_8(T_{HPG}, P_{PHG}) \tag{3.22}$$

The process of finding this solution is illustrated in figure 3.4. The intersection of the constant concentration line (where x_7=x_8) and T_{HPG} results in the maximum P_{HPG}. The corresponding maximum limit of T_{12} can be directly determined from P_{HPG}. P_{HPG} is determined by the pure liquid refrigerant outlet of the intermediate pressure generator (stream 12). So we can get $T_{12_{max}}$ from the pure ammonia line, as illustrated in figure 3.4. If T_{12} becomes higher than this limit, P_{HPG} will increase which in turn increases x_8 causing the high pressure generator to fail because x_8 becomes higher than x_4.

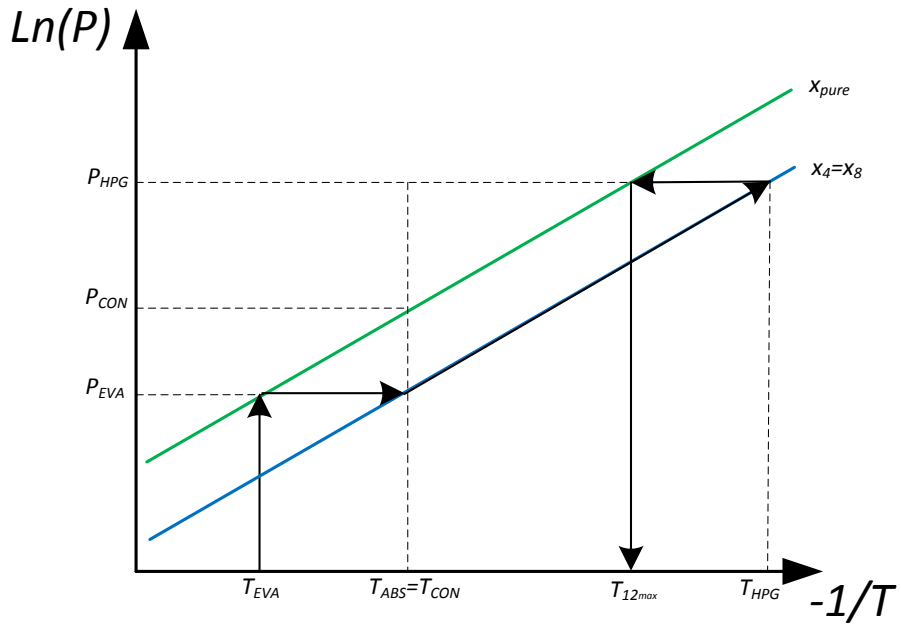

Figure 3.4: ln(P) - 1/T phase diagram to find the maximum temperature for T12. Resulting from the restriction of the high pressure generator. The green and blue line indicate the pure ammonia line and the solution concentration line, respectively. Horizontal lines are isobars, vertical lines are isotherms and isoconcentration lines are diagonal.

.

Restriction from the intermediate pressure generator The third restriction, equation 3.20, will give another minimum limit for T_{12}. The weak solution outlet concentration of the intermediate pressure generator, x_{15}, is dependent on P_{CON} and T_{15}. P_{CON} is fixed by T_{CON}, and x_{15} is determined by T_{15}, where T_{15} = T_{12} - 5K. The solution inlet concentration, x_{10} (where x_{10}=x_8), is determined by T_{HPG} and P_{HPG}. P_{HPG} is determined by T_{12}, so both concentrations are dependent on T_{12}. The limit at which the IPG can operate is at x_{10}=x_{15} (where x_{10}=x_8). The corresponding T_{12} can be found by iteratively solving equation 3.23, a physical interpretation is illustrated in figure 3.5. Because x_8 increases with increasing T_{12} and x_{15} decreases with increasing T_{12}, T_{12} should always be higher than the found limit.

$$x_8(T_{HPG}, P_{HPG}) = x_{15}(T_{15}, P_{CON}) \tag{3.23}$$

Before predicting the performance of the thermodynamic model, an analysis of the operating conditions is required. Tables 3.5 and 3.6 list the range of T_{12} for 9 ammonia-ionic liquid working pairs for a cooling and heating application, respectively. In the tables, two minima and one maximum for T_{12} are shown. To have a possible range for T_{12}, both minima must be lower than the maximum. Five of the nine working pairs cannot be operated at these conditions so limited or no possible working conditions are expected. The pairs with [Bmim][BF4], [Emim][BF4], [Emim][SCN] and [Mmim][DMP] show a small range of T_{12} which suggests that there is an operating range, but it is very limited.

3.4.2. Performance prediction

The previous chapter made clear that some of the working pairs in this cycle are not very flexible. From tables 3.5 and 3.6 one would expect [Bmim][BF4], [Emim][BF4], [Emim][SCN] and [Mmim][DMP] to be most flexible and have the highest COP for the cycle. Figure 3.6 shows the $COP_{cooling}$ for the working pairs at T_{ABS}=30°C, T_{CON}=30°C, T_{CON} and T_{EVA}=10°C for different T_{HPG}.

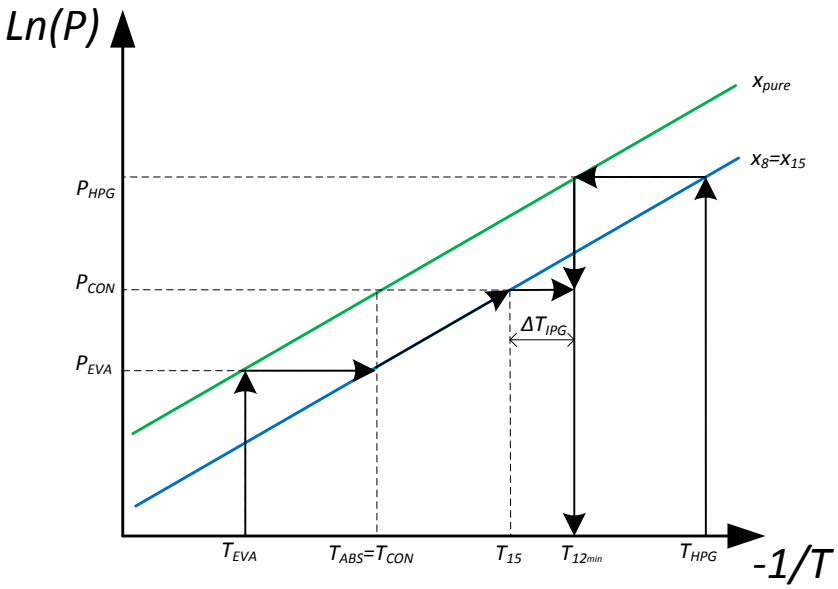

Figure 3.5: ln(P) - 1/T phase diagram to find a minimum temperature for T12. Resulting from the restriction of the intermediate pressure generator. The green and blue line indicate the pure ammonia line and the solution concentration line, respectively. Horizontal lines are isobars, vertical lines are isotherms and isoconcentration lines are diagonal.

These operating conditions are not realistic but give an opportunity to compare most of the ionic liquids. Seven out of the nine working pairs can operate at these conditions. All four ionic liquids that had a possible range for the conditions in tables 3.5 and 3.6 have the highest COP. The ionic liquid with the largest range of possible T_{12}, [Mmim][DMP], has the highest COP for most of the range. For two ionic liquids, [Hmim][BF4] and [Emim][EtOSO3] no T_{12} could be found to satisfy the energy balance, so they are not displayed in figure 3.6. The ILs [Bmim][PF6] and [Omim][BF4], which didn't show promise, did give a result, but they have a lower COP than the other four ILs. These results show that having a large range for T_{12} could be an indicator of better performance.

3.4.3. Performance prediction for cooling applications

The four best working pairs are selected for further investigation. For the operating conditions listed in table 3.5, the performance of the four working pairs is displayed in figure 3.7. As expected from the investigation of the range of T_{12} in table 3.5, [Mmin][DMP] has the largest operating range followed by [Bmin][BF4]. Out of the investigated ionic liquids, [Bmim][BF4] reaches the highest COP so its performance will be described in detail. In further investigations the COP and the pump power are calculated with equations 3.24-3.26. The densities used to calculate the pump power for the investigated absorber temperature range are listed in table 3.7.

$$COP_{cooling} = \frac{\dot{Q}_{EVA}}{\dot{Q}_{HPG} + \dot{W}_{PUMP}} \tag{3.24}$$

$$\dot{W}_{pump} = \frac{\dot{m}_4}{\rho_{sol}} \frac{(P_{HPG} - P_{EVA})}{\eta_{PUMP}} \tag{3.25}$$

$$\rho_{sol} = x_4 \rho_{NH_3} + (1 - x_4)\rho_{IL} \tag{3.26}$$

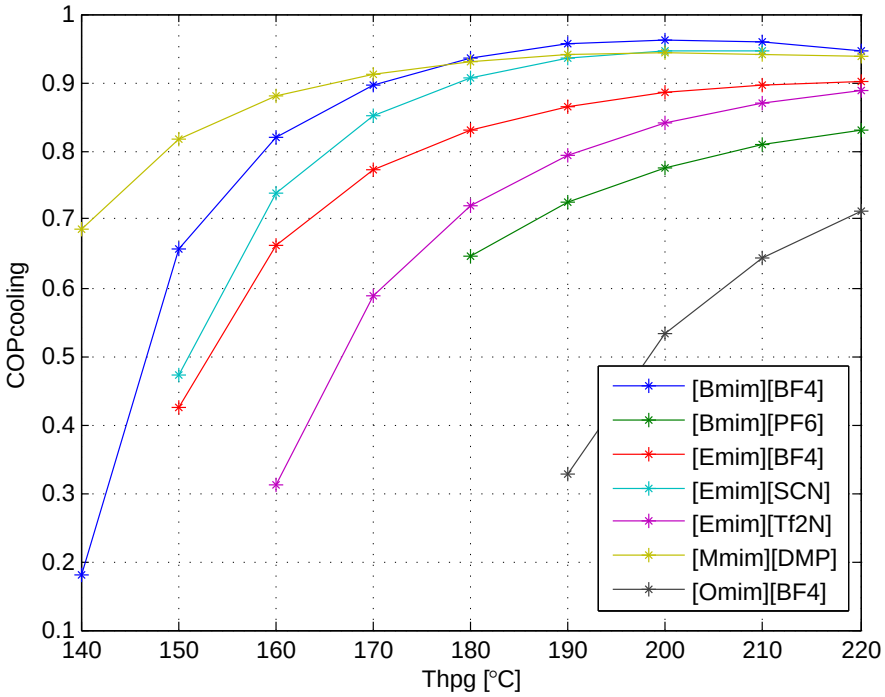

Figure 3.6: The COP of the double effect absorption cycle as a function of the driving temperature. For the conditions: T_{ABS} = T_{CON} = 30 °C and T_{EVA} = 10 °C using seven of the nine investigated ionic liquids. For the absorbents [Emim][EtOSO3] and [Hmim][BF4] no operating temperature could be found that did not violate a restriction.

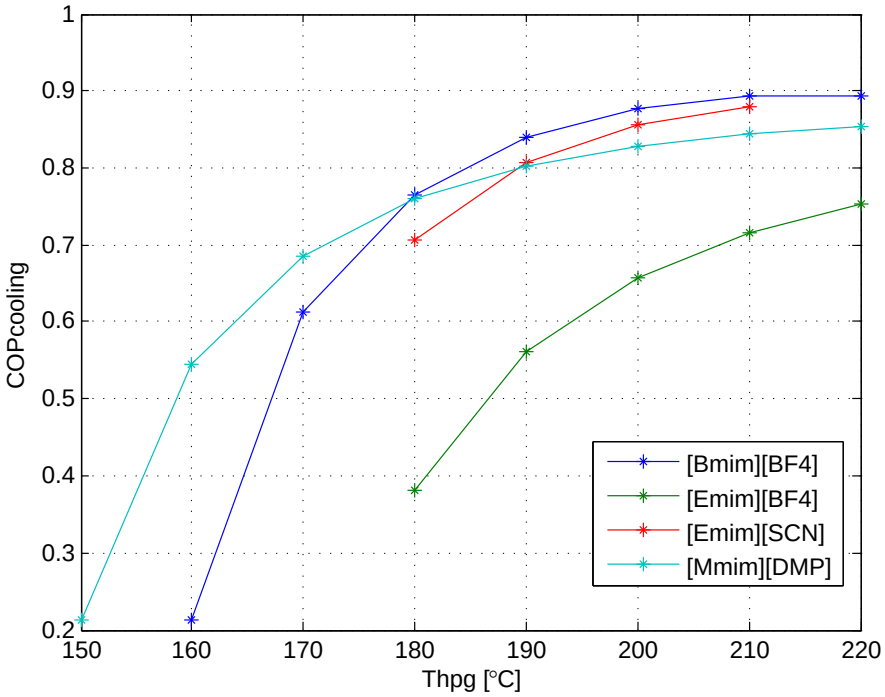

Figure 3.7: The COP of the double effect absorption cycle as a function of the driving temperature. For the conditions: T_{ABS} = T_{CON} = 40 °C and T_{EVA} = 5 °C using the four best performing ionic liquids as absorbent. The ionic liquid [Bmim][BF4] shows the best performance for most of the investigated temperature range.

Table 3.5: Range of T_{12} for a cooling application. Five out of the nine working pairs show no possible intermediate pressure generator refrigerant outlet temperature (T_{12}) for the operating conditions: T_{CON}=40°C, T_{ABS}=40°C, T_{HPG}=180°C and T_{EVA}=5°C. Based on the vapor liquid equilibrium data and their corresponding NRTL parameters, they would not be suitable.

Absorbent	$T_{12_{min1}}$ [°C]	$T_{12_{min2}}$ [°C]	$T_{12_{max}}$ [°C]	**Range** [K]
[Bmim][BF4]	92.5	103.1	109.7	6.7
[Bmim][PF6]	98.0	94.8	90.9	none
[Emim][BF4]	93.8	97.4	100.2	2.9
[Emim][EtOSO3]	92.7	81.3	68.6	none
[Emim][SCN]	95.9	105.5	111.7	6.3
[Emim][Tf2N]	98.1	97.0	95.2	none
[Hmim][BF4]	128.2	95.0	72.0	none
[Mmim][DMP]	87.9	98.6	110.7	12.1
[Omim][BF4]	105.9	92.9	79.8	none

Table 3.6: Range of T_{12} for a heating application Similar to the cooling application, five out of the nine working pairs show no possible intermediate pressure generator refrigerant outlet temperature (T_{12}) for the conditions: T_{CON}=T_{ABS}=45°C, T_{HPG}=180°C and T_{EVA}=10°C. Based on the vapor liquid equilibrium data and their corresponding NRTL parameters, they would not be suitable.

Absorbent	$T_{12_{min1}}$ [°C]	$T_{12_{min2}}$ [°C]	$T_{12_{max}}$ [°C]	**Range** [K]
[Bmim][BF4]	97.0	105.7	111.3	5.7
[Bmim][PF6]	102.4	98.6	94.2	none
[Emim][BF4]	98.5	100.9	102.8	1.9
[Emim][EtOSO3]	98.2	84.9	70.4	none
[Emim][SCN]	99.8	108.3	113.8	5.5
[Emim][Tf2N]	102.3	100.5	98.2	none
[Hmim][BF4]	129.3	98.7	76.7	none
[Mmim][DMP]	92.9	102.1	112.3	10.2
[Omim][BF4]	110.8	97.1	83.8	none

Figure 3.8 shows the COP of the cycle for different absorber and condenser temperatures using the ionic liquid [Bmin][BF4]. As expected, for lower absorber and condenser temperatures the system has a higher performance. This is because a higher condenser temperature gives a higher condenser pressure resulting in a higher concentration of stream 15, meaning less ammonia can be evaporated in the intermediate pressure generator. Increasing the absorber temperature results in lower strong solution concentration (stream 4) because higher temperatures give a lower ammonia concentration. A lower strong solution concentration gives a lower COP because there is less ammonia to be evaporated in the high pressure generator. For every absorber temperature there is a minimum and maximum T_{HPG} for which the cycle can run. If the temperature becomes lower than this limit, the restriction from equation 3.19 will be violated. That is, the concentration of the solution leaving the high pressure generator exceeds that of the entering solution. The maximum driving temperature is because of one the assumptions of the thermodynamic model, ammonia has to be at saturated conditions at stream 12, meaning that the temperature cannot exceed the critical point of ammonia at this point. Furthermore, there is an optimum T_{HPG} for every curve. If the absorber and condenser are connected in series with the external fluid, it is important to choose the best performing configuration. Figure 3.8 should be used to accomplish that. If the absorber exchanges heat with the environment at 40°C and the condenser at 30°C, for a T_{HPG} of 220°C, the COP is 0.84. Switching

Table 3.7: The densities of [Bmim][BF4] for the investigated absorber temperature range. The densities change less then 0.1% for the investigated pressure range and they are considered to be temperature dependent only. Experimental data is taken from Matkowska and Hofman [19].

T_{ABS} [°C]	**Density** $[kg/m^3]$
30	1198
35	1194.5
40	1191
45	1187.5

the condenser and absorber, so T_{ABS}=30°C and T_{CON}=40°C, results in the same COP. However, in accordance with figure 3.8 for a lower driving heat (e.g. T_{HPG}=180°C), having the absorber solution oulet at a lower temperature than the condenser outlet can improve the performance by 10%.

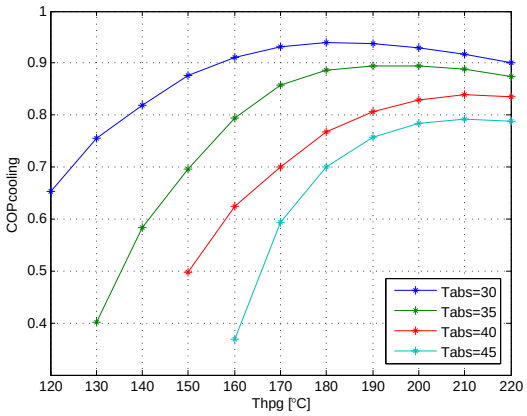

(a) The COP for the given conditions and T_{CON} = 30°C

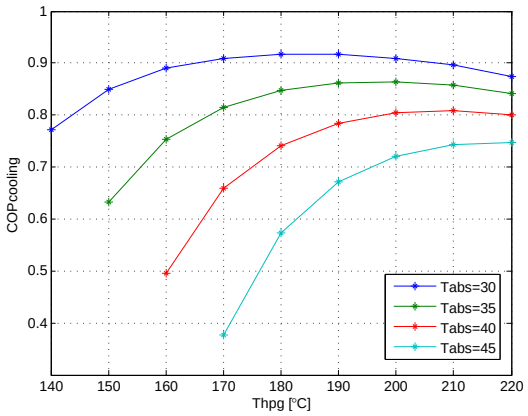

(b) The COP for the given conditions and T_{CON} = 35°C

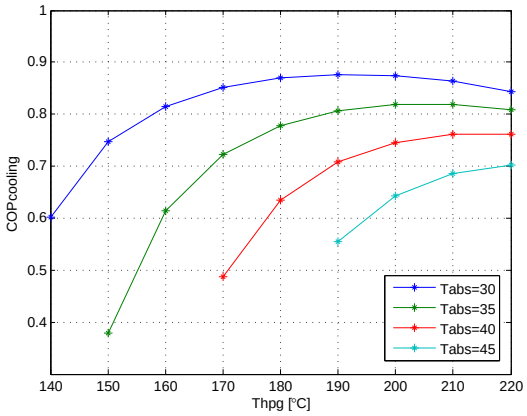

(c) The COP for the given conditions and T_{CON} = 40°C

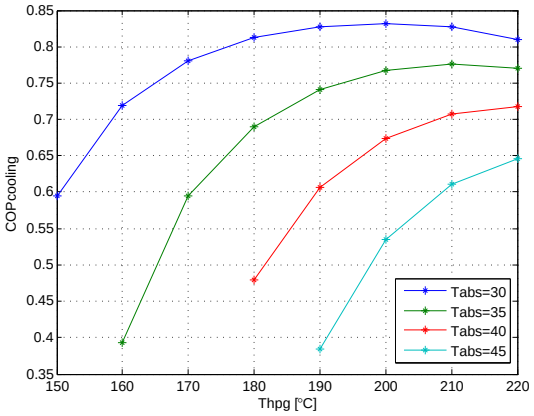

(d) The COP for the given conditions and T_{CON} = 45°C

Figure 3.8: The COP of the double effect absorption cycle as a function of the driving temperature for different condenser and absorber temperatures. For the condition T_{EVA} = 5 °C using [Bmim][BF4] as absorbent. The diagram can be used as a guide for selecting the best way to connect the absorber and condenser with the external fluid to exchange heat.

Figure 3.9 shows the influence of the evaporation temperature on the COP of the double-effect absorption cycle. The trend shows that having a higher evaporation temperature increases the performance of the cycle. Furthermore, there seems to be an optimum temperature for every curve. For lower evaporation temperatures the optimum T_{HPG} cannot be reached because the critical temperature of ammonia will be exceeded. Having a high evaporation temperature results in a high evaporator pressure. Consequently, the strong solution concentration will become higher, so more ammonia can be evaporated in the high pressure generator. The cycle seems to be suitable for cooling applications down to approximately -5 °C because there is a realistic range of operation.

The effect of the driving temperature on the concentration of the solution through the cycle is shown in figure 3.10. As expected, the highest concentration level is constant because this is independent of the driving temperature. Both the intermediate and the weakest concentration levels decrease with increasing temperature. For instructive purposes, the lower limit of the driving temperature is exceeded to see what will happen to the concentrations. Predictably, restrictions from equations 3.18-3.20 are violated and the strong concentration gets surpassed by the weakest and intermediate concentration.

Having a large concentration difference increases the cooling load but at the same time this requires more heat input in the high pressure generator. This effect can clearly be seen in figure 3.11.

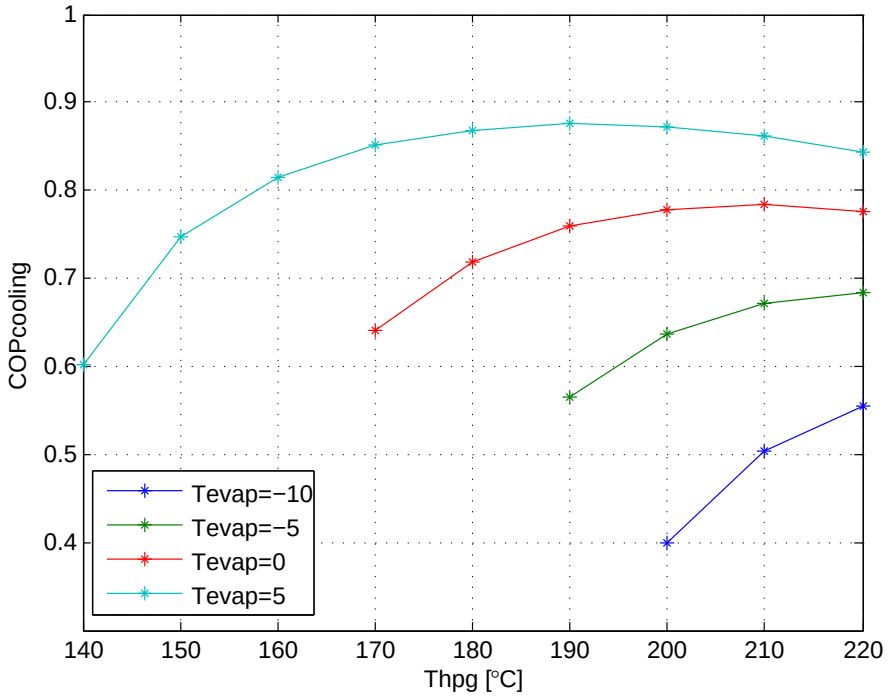

Figure 3.9: The COP of the double effect absorption cycle as a function of the driving temperature for different evaporation temperatures. For the conditions: T_{CON} = 40 °C, T_{EVA} = 30 °C, using [Bmim][BF4] as absorbent. For lower evaporation temperatures the minimum temperature of the high pressure generator solution outlet becomes very high, this narrows down the scope of possible applications.

The driving heat and evaporator heat increase at approximately the same rate with increasing driving temperature. Furthermore, the pump power also increases because the pressure difference becomes larger with increasing driving temperature.

All the properties [Bmim][BF4] and ammonia at all the points in the cycle for the conditions T_{ABS}=30, T_{CON}=40 °C, T_{EVA}=5 °C and T_{HPG}=220 °C are listed in table 3.9. The COP and heat flows are listed in table 3.10. The results show that it is necessary to take the pump power into account, as this can decrease the performance up to 10%. The performance is better than the ammonia water working pair in the double-effect cycle for evaporation temperatures at 0 °C or below but higher driving temperatures are needed, as can be seen in table 3.8. However, for evaporation temperatures above 0 °C, the lithium bromide working pair reaches a higher COP.

Table 3.8: Performance comparison of the best performing ionic liquid based working pair and ammonia and water. In the double-effect absorption cycle in series configuration. As can be seen, the ionic liquid reaches a higher COP than water as absorbent but the required high pressure generator temperature is higher.

Symbol	Ammonia / [Bmim][BF4]	Ammonia / water
T_{EVA}	0 °C	0 °C
T_{ABS}=T_{CON}	30 °C	30 °C
T_{HPG}	194 °C	138 °C
COP	0.869 [-]	0.829 [-]

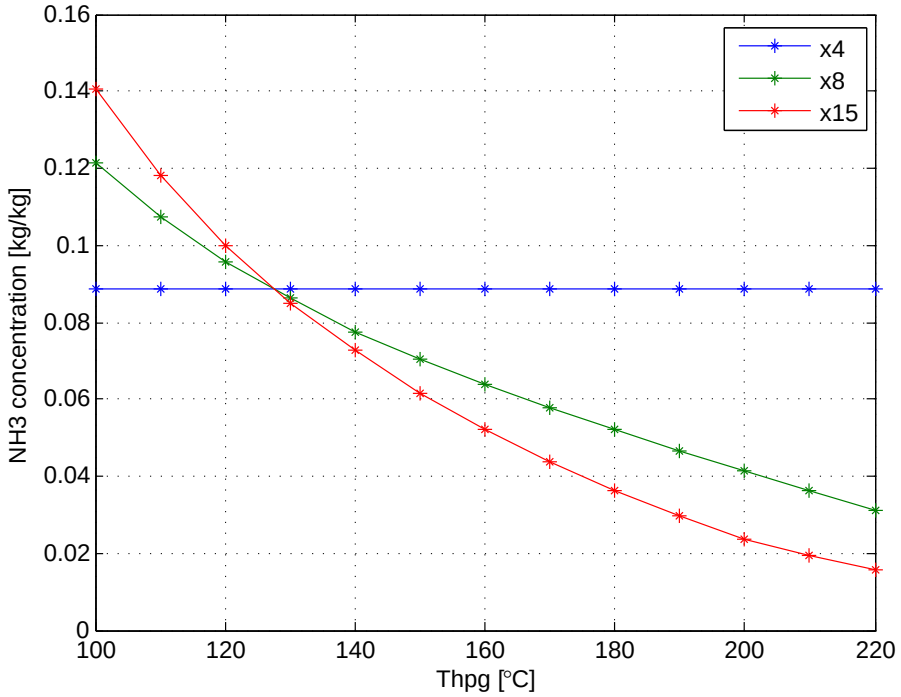

Figure 3.10: The three ammonia concentration levels in the solution flow of the double-effect absorption cycle as a function of the driving temperature. For the conditions: T_{ABS} = 40 °C, T_{CON} = 30 °C and T_{EVA} = 5 °C using [Bmim][BF4] as absorbent. The minimum operating temperature can be seen around 130 °C, below this limit the restrictions are violated and the cycle would not work.

Table 3.9: State properties of the double effect absorption cycle during cooling using [Bmim][BF4]. For the conditions: T_{ABS} = 30°, T_{CON} = 40 °C, T_{EVA} = 5 °C and T_{HPG} = 220 °C.

Point	Flow [kg/s]	Temp. [°C]	Conc.[kg/kg]	Pressure [bar]	Enthalpy [kJ/kg]	Quality [kg/kg]
1	0.0742	40.0000	1.0000	15.5517	535.0010	0.0000
2	0.0742	5.0000	1.0000	5.1571	535.0010	0.1344
3	0.0742	5.0000	1.0000	5.1571	1612.3436	1.0000
4	1.0000	30.0000	0.0886	5.1571	98.0216	0.0000
5	1.0000	37.0250	0.0886	107.2471	108.4027	0.0000
6	1.0000	103.8542	0.0886	107.2471	245.3708	0.0000
7	1.0000	196.4601	0.0886	107.2471	450.5271	0.0100
8	0.9408	220.0000	0.0312	107.2471	450.4204	0.0000
9	0.9408	108.8542	0.0312	107.2471	232.3461	0.0000
10	0.9408	107.5586	0.0312	15.5517	232.3461	0.0020
11	0.0592	196.4601	1.0000	107.2471	1875.6409	1.0000
12	0.0592	129.1100	1.0000	107.2471	1115.2148	0.0000
13	0.0592	40.0000	1.0000	15.5517	1115.2148	0.5276
14	0.0150	107.5586	1.0000	15.5517	1827.1822	1.0000
15	0.9258	124.1200	0.0155	15.5517	255.1930	0.0000
16	0.9258	42.0250	0.0155	15.5517	107.2438	0.0000
17	0.9258	42.0134	0.0155	5.1571	107.2438	0.0000

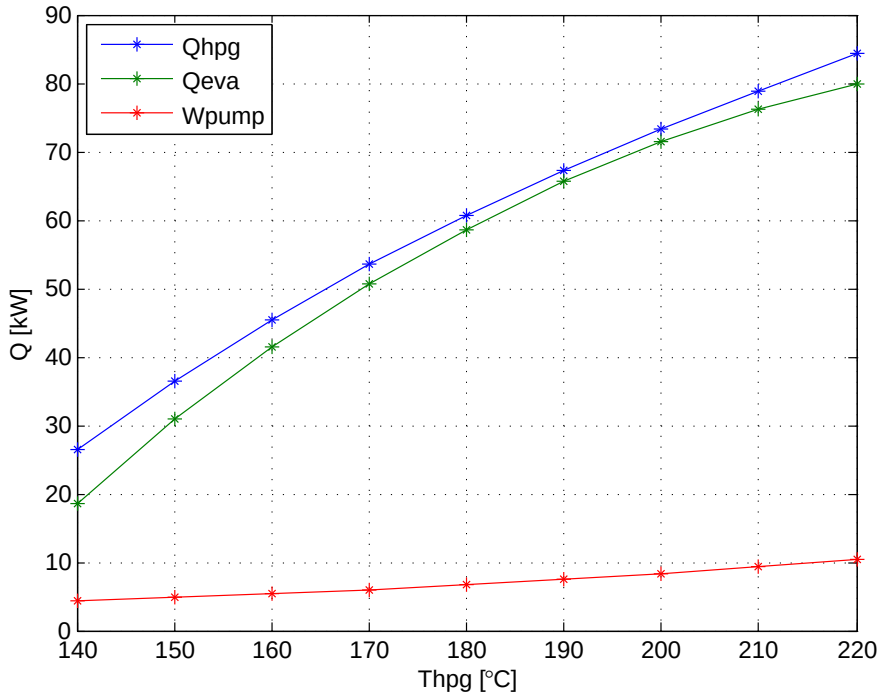

Figure 3.11: The heat flow of the evaporator, the high pressure generator and pumping power of the double effect absorption cycle as a function of the driving temperature. For the conditions: T_{ABS} = 40 °C, T_{CON}=30 °C and T_{EVA} = 5 °C using [Bmim][BF4] as absorbent. For lower temperatures it can be seen that the pump power has a large contribution, the power needed for the pump is almost 25 % of the cooling power at 140 °C.

Table 3.10: Results obtained from the model for a cooling application using [Bmim][BF4]. For the conditions: T_{ABS} = 30, T_{CON} = 40 °C, T_{EVA} = 5 °C and T_{HPG} = 220 °C.

Symbol	Value	Unit	Description
Q_{EVA}	79.96	[kW]	Heat flow in the evaporator
Q_{ABS}	120.93	[kW]	Heat flow in the absorber
Q_{CON}	53.73	[kW]	Heat flow in the condenser
Q_{HPG}	84.32	[kW]	Heat added to the high pressure generator
Q_{IPG}	45.05	[kW]	Heat exchanged in the intermediate pressure generator
W_{PUMP}	10.38	[kW]	Pump power
$COP_{cooling}$	0.84	[-]	COP for cooling

3.4.4. Performance prediction for heating applications

Three ionic liquid absorbents are investigated for the performance prediction of a heating application. The performance of the workings pairs is shown in figure 3.12. As expected from the investigation of the range of T_{12} in table 3.6, [EMIM][SCN] has the smallest operating range. Furthermore, for the heating application the performances of the working pairs are much closer to each other at higher driving temperatures. The ionic liquid [Bmin][BF4] reaches the highest COP again. The state properties and the results of [Bmin][BF4] during a heating application for the conditions T_{EVA}=10°, T_{CON}=45°, T_{ABS}=35° and T_{HPG}=210° are shown in tables 3.11 and 3.12. The pumping power is included in these results and the COP is calculated by equation 3.27

$$COP_{heating} = \frac{\dot{Q}_{ABS} + \dot{Q}_{CON}}{\dot{Q}_{HPG} + \dot{W}_{PUMP}} \tag{3.27}$$

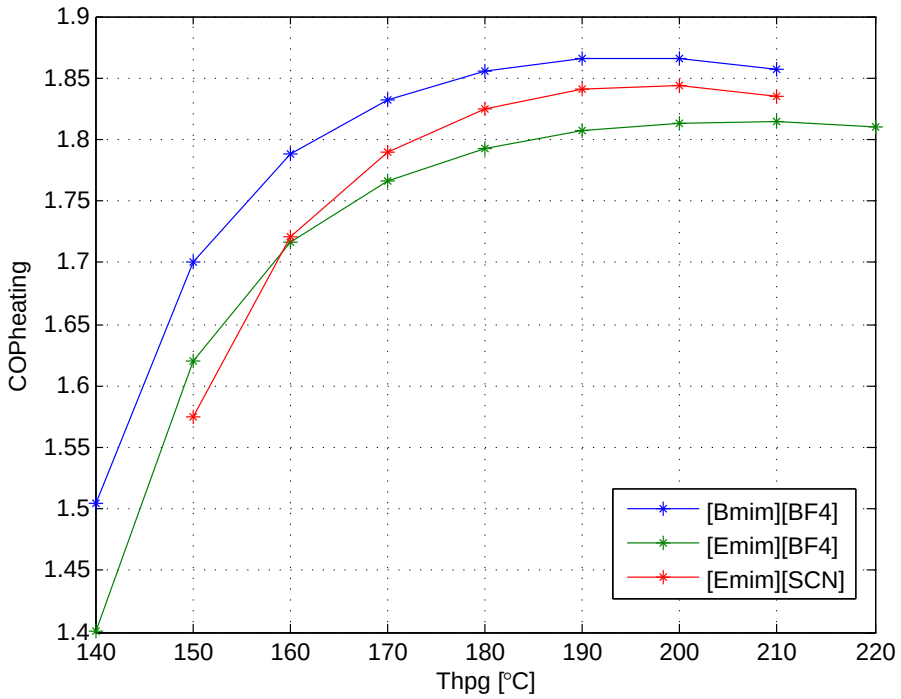

Figure 3.12: The COP of the double effect absorption cycle as a function of the driving temperature. For the conditions: T_{ABS} = 35, °T_{CON} = 45, °C and T_{EVA} = 10 °C using three of the ionic liquids as absorbent. The ionic liquid [Bmim][BF4] shows the best performance for the investigated temperature range.

Table 3.11: State properties of the double effect absorption cycle during a heating application using [Bmim][BF4]. At conditions: T_{ABS} = 35, °T_{CON} = 45, °C and T_{EVA} = 10 °C and T_{HPG} = 210 °C.

Point	Flow [kg/s]	Temp. [°C]	B	Pressure [bar]	Enthalpy [kJ/kg]	Quality [kg/kg]
1	0.0728	45.0000	1.0000	17.8240	559.8521	0.0000
2	0.0728	10.0000	1.0000	6.1497	559.8521	0.1377
3	0.0728	10.0000	1.0000	6.1497	1617.0582	1.0000
4	1.0000	35.0000	0.0943	6.1497	108.6315	0.0000
5	1.0000	41.6348	0.0943	99.9576	118.2570	0.0000
6	1.0000	101.9178	0.0943	99.9576	243.3103	0.0000
7	1.0000	187.7483	0.0943	99.9576	436.8427	0.0087
8	0.9441	210.0000	0.0407	99.9576	437.4713	0.0000
9	0.9441	106.9178	0.0407	99.9576	232.4781	0.0000
10	0.9441	105.9840	0.0407	17.8240	232.4781	0.0010
11	0.0559	187.7483	1.0000	99.9576	1858.6324	1.0000
12	0.0559	125.1500	1.0000	99.9576	1064.2846	0.0000
13	0.0559	45.0000	1.0000	17.8240	1064.2846	0.4689
14	0.0169	105.9840	1.0000	17.8240	1815.7515	1.0000
15	0.9272	120.1600	0.0232	17.8240	251.6178	0.0000
16	0.9272	46.6348	0.0232	17.8240	116.7479	0.0000
17	0.9272	46.6211	0.0232	6.1497	116.7479	0.0000

Table 3.12: Results obtained from the model for a heating application using [Bmim][BF4]. For the conditions: T_{ABS} = 35, T_{CON} = 45 °C, T_{EVA} = 10 °C and T_{HPG} = 210 °C.

Symbol	Value	Unit	Description
Q_{EVA}	76.95	[kW]	Heat flow in the evaporator
Q_{ABS}	117.32	[kW]	Heat flow in the absorber
Q_{CON}	49.40	[kW]	Heat flow in the condenser
Q_{HPG}	80.08	[kW]	Heat added to the high pressure generator
Q_{IPG}	44.41	[kW]	Heat exchanged in the intermediate pressure generator
W_{PUMP}	9.63	[kW]	Pump power
$COP_{heating}$	1.86	[-]	COP for heating

3.4.5. Influence of the design parameters on the performance

Figure 3.13 shows the influence of the pinch temperature of HEX1, HEX2 and the intermediate pressure generator on the performance. From the figure it can be concluded that the pinch temperatures of the heat exchangers have a stronger effect on the performance than that of the intermediate pressure generator. If the pinch temperature increases in HEX1 and HEX2, the temperature of the solution entering the high pressure generator will be lower. In that case, the high pressure generator will require more heat input in order to have the same outlet temperature which reduces the performance, explaining the negative slope in figure 3.13.

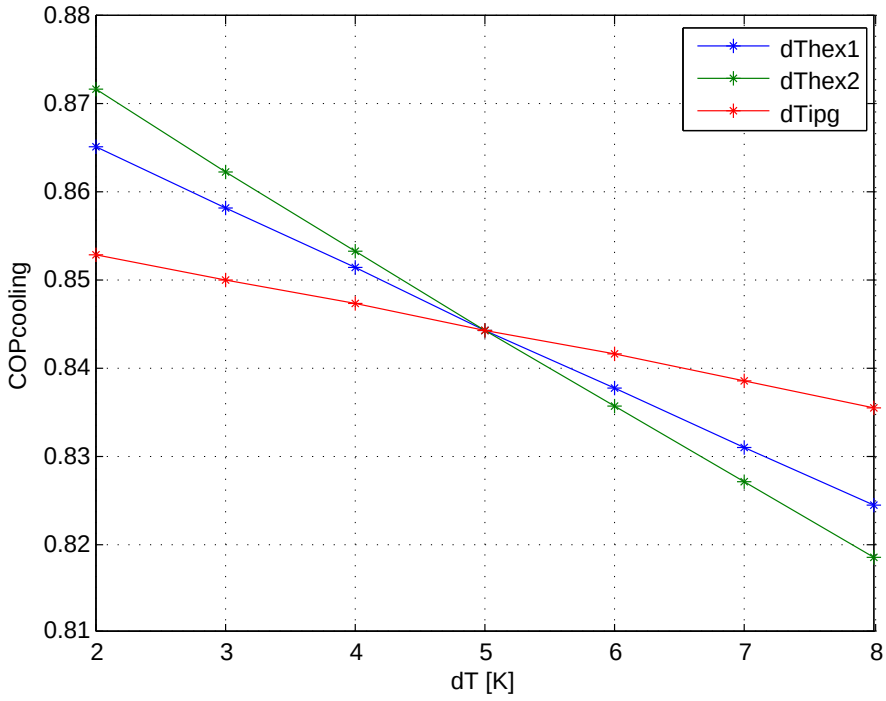

Figure 3.13: The influence of the pinch temperature. In the intermediate pressure generator and the first and second solution heat exchangers on the COP of the cycle as a function of the high pressure generator solution outlet temperature. For the conditions: T_{ABS} = 40 °C, T_{CON} = 30 °C and T_{EVA} = 5 °C using [Bmim][BF4] as absorbent.

3.5. Recommendations

3.5.1. Conclusions

- The double-effect absorption cycle using ammonia and water with rectifiers for the conditions T_{ABS}=30 °C, T_{CON}=30 °C and T_{EVA}=0 °C has a COP of 0.83, whereas ammonia and [Bmim][BF4] has a COP of 0.87. For lower evaporation temperatures, this performance difference becomes even larger. Additionally, using ionic liquid as absorbent has the preference because there is no need for rectifiers, thus it is a much simpler construction.
- The pump power has a strong influence on the performance. For some cases, the required pump power can decrease the COP with 10 %. This is because there is a large pressure difference compared to the ammonia water working pair which would be a design challenge.
- For evaporation temperatures above 0 °C, the performance of the double-effect cycle in series configuration using the investigated ionic liquids cannot compete with the performance of the lithium bromide and water working pair.

3.5.2. Recommendations

- In this research, the mixing enthalpy is assumed to be zero. In reality, this is not zero and the effect on the performance of the cycle should be investigated.
- The effect of the viscosity of the ionic liquid ammonia mixture on the pump power, and thus the performance on the cycle, should be investigated.

4

Method to determine the excess enthalpy for ionic liquid and ammonia mixtures

4.1. Introduction

In this chapter, a method is proposed to measure the excess enthalpy of an ammonia and ionic liquid mixture. First, the theory on excess properties will be explained and the experimental method is described. A way to validate the method is proposed and illustrated by an example using ammonia and water. Lastly, the recommendations are presented.

4.2. Theory

4.2.1. Excess properties

An excess property, M^E, is the difference between the actual property of a solution and the property of the ideal solution at a given temperature, pressure and composition:

$$M^E = M - M^{id} \tag{4.1}$$

For a binary mixture, the property of mixing is defined as:

$$M^E = M - x_a M_a - x_b M_b \tag{4.2}$$

Where the subscripts a and b denote the pure components.

4.2.2. Mixing two liquids

If two pure liquids are mixed under the condition of constant pressure, the change in the total enthalpy is the excess enthalpy. In this case, the heat released or absorbed by the two liquids during mixing can be measured directly. Then the excess enthalpy can be calculated by [27]:

$$H^E = \frac{Q}{m} \tag{4.3}$$

Where Q is the heat released or absorbed and m the total mass of the sample.

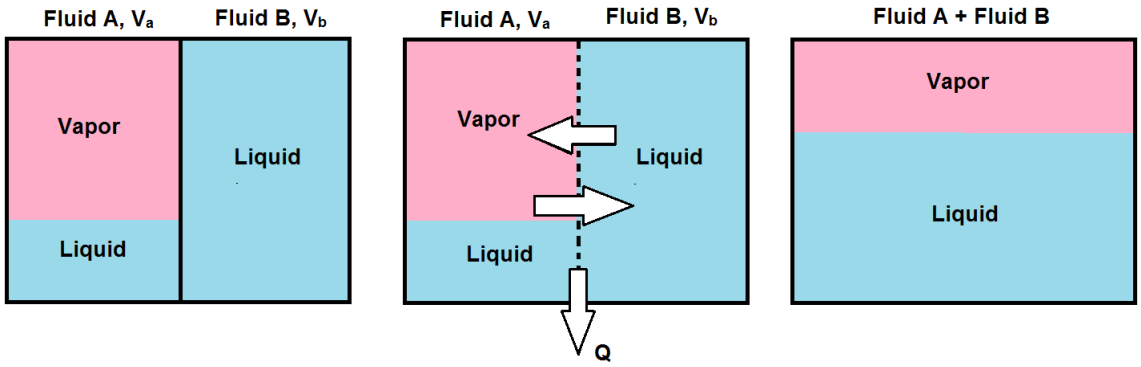

Figure 4.1: The mixing process of two fluids in different phases. From left to right: Two pure fluids separated by a wall, Two pure fluids mixing after removing the wall and releasing or absorbing heat, Two-phase equilibrium formed of fluid A and B

.

4.2.3. Mixing a liquid with two-phase volume

If we consider the system as illustrated in figure 4.1, where on the left side we have a two-phase region in equilibrium of pure fluid A, and on the right side a pure liquid B which are separated by a non-permeable wall. The system is at uniform and constant temperature T and pressure P. If the non-permeable wall is removed, the two-phase region and the liquid will start mixing and a new equilibrium is formed with a new pressure and temperature. And again, the heat released or absorbed by the system can be measured directly, from which the excess enthalpy can be calculated. However, in this case the gas phase of fluid A has an effect on the excess enthalpy due to condensation/evaporation and absorption/desorption to or from the liquid phase.

4.2.4. Ionic liquid and ammonia

Now if we think of the case where we would mix ammonia with an ionic liquid we can make some assumptions. In a two phase equilibrium of ammonia and ionic liquid we can assume that the vapor pressure of the ionic liquid is negligible and ammonia has a high solubility in ionic liquid [36]. So if we consider the system illustrated by figure 4.1, after taking away the non-permeable wall we can assume that a part of the ammonia will get absorbed by the ionic liquid and that the vapor phase is pure ammonia. The mole-based enthalpy of mixing can be determined by:

$$\bar{h}^E = \frac{Q}{n_{IL} + n_{NH_3,l}} \tag{4.4}$$

Where Q is the heat released or absorbed by the system during mixing and $n_{NH_3,l}$ is the amount of ammonia absorbed by the ionic liquid. Or the mass-based enthalpy of mixing by:

$$h^E = \frac{Q}{m_{IL} + m_{NH_3,l}} \tag{4.5}$$

4.3. Method

4.3.1. Introduction

This method measures the mixing enthalpy for two fluids at a certain pressure, temperature and composition. Before mixing, the fluids can be in single phase or in two-phase. The method makes use of two connected volumes, each consisting of a pure fluid, that are connected by a valve that

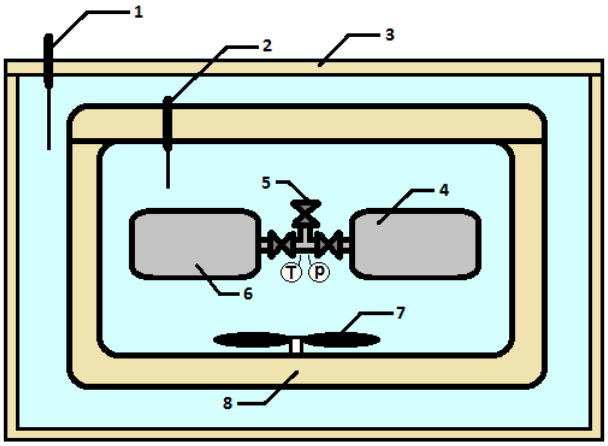

Figure 4.2: A schematic illustration of the set-up with its main components. Following the ordering of the illustration the components are: 1. Pt-100 temperature sensor, 2. Pt-100 temperature sensor , 3. Thermostatic bath filled with water, 4. Ammonia sample, 5. Valve, 6. Ionic liquid sample, 7. Mixer, 8. Insulated box filled with water.

.

is initially closed. By means of a thermostatic bath the samples (or volumes) will be brought to the desired temperature, after which the valve will be opened. The fluids will start mixing and the heat released or absorbed by this mixing process will be measured, from which the excess enthalpy can be calculated. The final pressure and composition can be determined by a pressure sensor inside the connected samples.

Set-up The set-up consists of the following equipment:

- Temperature sensors
- Thermostatic bath filled with water
- Coupled ammonia / ionic liquid sample
- Mixer
- Insulated box filled with water

The equipment will be set-up as illustrated in figure 4.2. As can be seen, the insulated box with the connected samples is submerged into a thermostatic bath. Initially, the insulated box will be open, so all the water can flow freely into the box. The thermostatic bath will be set to the chosen experiment temperature. By waiting long enough, the water and coupled samples will reach this temperature. Then, the valves connecting the cylinder samples will be opened and the insulated box will be closed quickly. This will form a closed system, consisting of the insulated box with the water and coupled sample cylinders inside. The fluids from both sample cylinders will start mixing through the connecting T-piece from left to right and vice versa. During this mixing process the connected cylinders will exchange heat with the surrounding water because of the excess enthalpy. In the case of an exothermic process, the temperature of the water in the insulated box will increase. Using the temperature increase of the water, the heat released by the samples can be calculated. To determine the total amount of water inside the insulated box, the box and samples have to be measured with and without water inside. Before, during and after the mixing process the temperature and pressure of the fluids inside the samples will be monitored.

4.3.2. Preparation of samples

To accurately prepare the ammonia and ionic liquid samples the following equipment is required:

- Vacuum pump
- Sample cylinders
- Connecting T-piece
- Pressurized ammonia tank
- Pressure regulating valve
- Pressure & temperature sensor

The mass of these parts will be measured. Then, the vacuum pump, the connecting T-piece and the pressurized ammonia tank are connected as in figure 4.3. The connecting T-piece and the sample cylinder are vacuumized using the vacuum pump to ensure there is no air inside. Now the sample can be filled with ammonia by setting the pressure regulating valve to the desired pressure and opening the pressurized ammonia tank. After the sample is filled with ammonia, the sample cylinder can be disconnected and weighed again, so we know exactly how much ammonia is in it. This procedure will be followed to prepare multiple ionic liquid and ammonia samples with different quantities inside. Once the samples have been made, they can be connected using the connecting T-piece to make ammonia and ionic liquid sample couples, as can be seen in figure 4.4. The valves will prevent the pure fluids from mixing. The vacuum pump and pressurized ammonia tank are available in the P&E lab of the TU Delft. The connecting T-pieces, sample cylinders and valves can be ordered from Swagelok.

4.3.3. Determination of the final composition

To determine the amount of ammonia absorbed by the ionic liquid, the vapor pressure and temperature have to be measured before and after mixing. To find the final concentration of the liquid phase x_{NH3} we follow the iterative loop illustrated in figure 4.5. An initial guess of the ammonia absorbed by the ionic liquid, $m_{NH3,l}$, has to be made. With this initial guess, the volume of the liquid phase can be determined by:

$$V_l = \frac{m_{IL}}{\rho_{IL}(T,P)} + \frac{m_{NH_3,l}}{\rho_{NH_3,l}(T,P)} \tag{4.6}$$

Where the densities can be found from NIST's Refprop database [17] and BOULDER website [22]. The excess volume has not been taken into account as this has been estimated to be less than 0.1%. The total volume is known so the volume of the gas phase can be calculated:

$$V_v = V_{tot} - V_l \tag{4.7}$$

With the volume of the gas phase and the density of ammonia, the amount of ammonia that is left in the gas phase can be calculated by:

$$m_{NH_3,v} = \rho_g(T,P)V_v \tag{4.8}$$

The total amount of ammonia is known, so the new calculated mass absorbed by the liquid and the error are:

$$m_{NH_3,l} = m_{NH_3,tot} - m_{NH_3,v} \tag{4.9}$$

$$Error = \frac{m_{NH_3,l_{guess}}}{m_{NH_3,l_{calc}}} \tag{4.10}$$

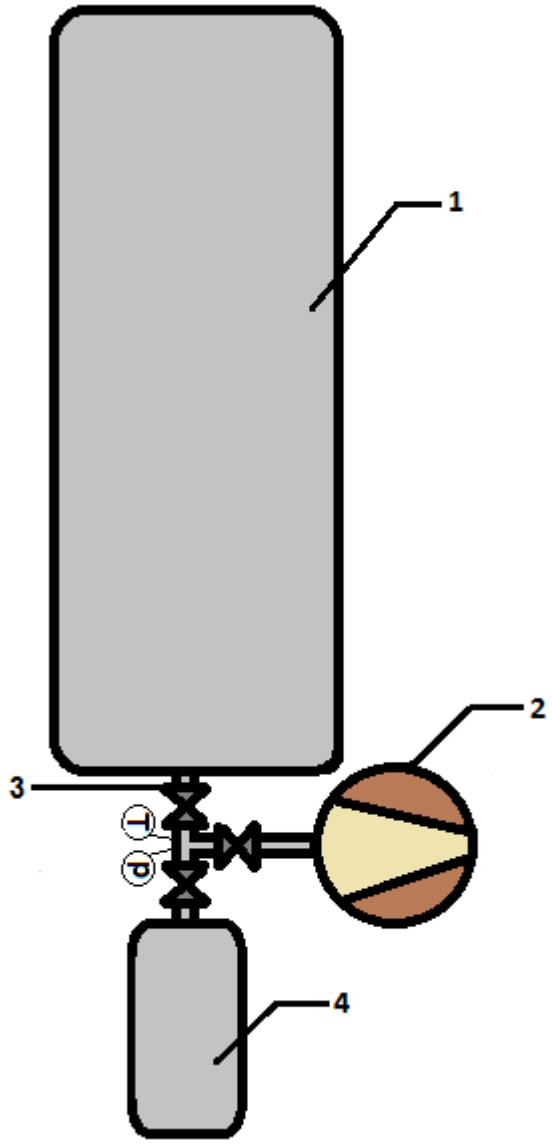

Figure 4.3: The set-up for filling the sample cylinders. Following the ordering of the illustration the components are: 1. Pressurized Ammonia tank, 2. Vacuum pump, 3. Pressure regulated valve, 4. Ammonia sample cylinder

.

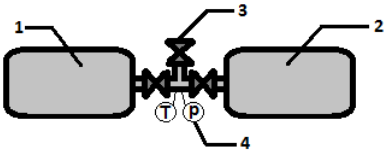

Figure 4.4: A schematic illustration of the connected samples. Following the ordering of the illustration the components are:1. Ammonia sample, 2. Ionic liquid sample, 3. Valve, 4. Connecting T-piece

.

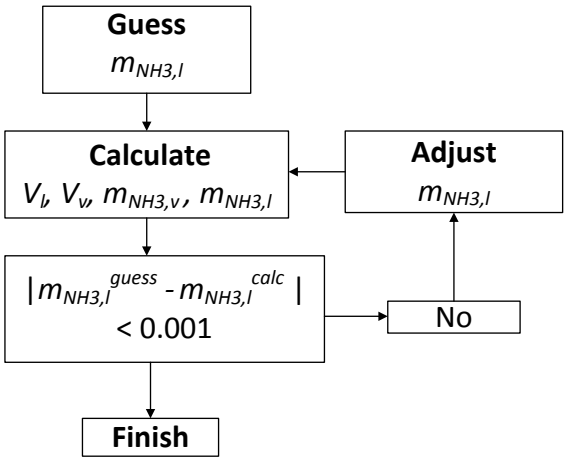

Figure 4.5: Iterative loop to determine the absorbed amount of ammonia in the liquid phase. The value of the amount of ammonia absorbed into the liquid is needed to calculate the excess enthalpy. The equations and iterative loop are solved using the software package Matlab.

.

Table 4.1: The conditions and properties of the example experiment. Conditions have been chosen to suit available equipment in the P&E lab, any other conditions can be chosen for these validations.

	Value	**Unit**	**description**
T_{exp}	273	[K]	Experiment temperature
P_{samp}	9	[Bar]	Pressure inside the connected sample
m_{NH_3}	0.3051	[kg]	Mass of ammonia inside the 500 ml sample
m_{H_2O}	0.2496	[kg]	Mass of water inside the 250 ml sample
x_{NH_3}	0.5499	[kg/kg]	Concentration of ammonia in the sample
h_{NH_3}	438.2	[kJ/kg]	Enthalpy of pure ammonia in the sample
h_{H_2O}	84.75	[kJ/kg]	Enthalpy of pure water in the sample
h	18.63	[kJ/kg]	Actual enthalpy of the mixture
$m_{H_2O,box}$	8.250	[kg]	Mass of the water inside the insulated box

Once the guessed value and the calculated value are close enough, the final concentration of the liquid phase can be calculated:

$$x_{NH3} = \frac{m_{NH_3,l}}{m_{NH_3,l} + m_{IL}} \tag{4.11}$$

4.4. Validation

To validate the set-up, the described method should be followed to determine the excess enthalpy of, e.g., ammonia and water. The results should be compared with values from NIST's REFPROP database. A practical example using readily available equipment and materials is shown below. In this example liquid ammonia and water will be mixed. The P&E lab has a thermostatic bath of 30x20x15 cm and sample cylinders of 250 ml and 500 ml can be ordered from Swagelok. Then, the method can be followed for the conditions and properties listed in table 4.1.

With these conditions, and using the REFPROP database, the heat released by the mixing process

Table 4.2: Results of the example experiment for the validation of the method. The results of the experiment for the conditions and properties listed in table 4.1. From the temperature rise, the excess enthalpy can be determined

	Value	Unit	Description
Q_{rel}	144.5	[kJ]	Heat released during mixing process
h^E	260.5	[kJ/kg]	Excess enthalpy
ΔT_{box}	4.17	[K]	Temperature rise of the water inside the insulated box

can be calculated with:

$$Q_{rel} = m_{tot}h - m_{NH_3}h_{NH_3} - m_{H_2O}h_{H_2O} \tag{4.12}$$

Then, the excess enthalpy of the ammonia water mixture can be calculated with:

$$h^E = \frac{Q_{rel}}{m_{tot}} \tag{4.13}$$

For the given conditions and volumes, the temperature rise should be close to the value listed in table 4.2.

4.5. Recommendations

In this chapter, a method to measure the excess enthalpy of two fluids at a certain temperature, pressure and composition has been described. The calculation procedure and needed components to do the measurements are given. Furthermore, an easy way to validate the method, using a mixture of ammonia and water, is described. Topics for further research are:

- The T-piece connecting the samples might interfere with the mixing process of the two fluids. This could cause the mixing process to be too slow. A magnetic stirrer inside the connected samples could prevent this from happening.
- Research on the influence of the propeller on the temperature of the water inside the insulated box should be conducted.
- In case of mixing a two-phase fluid with a one-phase fluid, the pressure inside the connected sample can change. The influence of a pressure change on the excess enthalpy should be investigated.

5

Case study: Dutch trawler fishing vessel

5.1. Introduction

Diesel engine combustion produces pollutants like SO_x and NO_x and approximately 3.3% of global CO_2 emissions are caused by shipping [10]. The refrigeration plant on fishing ships is the largest electricity consumer onboard. It is therefore logical to find ways to reduce the primary energy used for refrigeration. On board of a fishing vessel the main engine is a source of high temperature waste heat through the exhaust gas. The heat stored in this gas can be converted into cooling power to refrigerate the fish. The combination of a high temperature heat source and the need for cooling on fishing vessels present the perfect circumstances for absorption refrigeration.

Figure 5.1: A typical trawler fishing vessel.

5.2. Demand

The studied ship is a trawler fishing vessel which is mainly used to catch mackerel and herring. In order to cool and freeze the fish on-board, the vessel is equipped with three different refrigeration plants. The biggest energy consumers are the refrigerated seawater system (RSW), the chilled water plant (CWP) and the freezing plant. The chilled water plant is designed to cool down 47 m^3/h of seawater with a temperature of 32 °C to a temperature of -1 °C. This plant makes use of two screw compressors with a combined cooling power capacity of 1760 kW. The chilled water plant is turned on most of the time. The refrigerated seawater plant is designed to pre-cool fish to a temperature of 0 °C. It also makes used of two screw compressors with a combined cooling capacity of 2828 kW. Furthermore, the freezing plant is used to freeze mackerel and herring. It has the capacity to freeze 400 tons of mackerel or 460 tons of herring per 24 hours while maintaining the temperature of the holds at -30 °C using 10 screw compressors. The freezing plant has an effective cooling capacity of 2400 kW. Table 5.1 lists when each refrigeration plant is turned on for every operating mode. Table 5.2 lists the cooling demands and the cooling temperatures. The vessel requires a total of 6982 kW cooling power.

Table 5.1: The refrigeration plants and when they are turned on for the different operating modes.

	RSW	**CWP**	**Freezing plant**
Fishing with production	On	On	On
Fishing without production	On	Off	Off
Sailing to fishing zone and tracking down fish	On	Off	Off
Retrieving or placing nets, pumping fish on board	On	On	On
Out of order or unloading fish	Off	Off	Off

Table 5.2: The cooling power and electric power consumption of the three refrigeration plants.

	Cooling power demand [kW]	**Electric power consumption [kW]**	**Cooling temperature [°C]**	$T_{ABS} = T_{CON}$ **[°C]**
RSW	2828 (2x 1414)	1068	-1	-6
CWP	1760 (2x 880)	577	-1	-6
Freezing plant	2400	4610	-30	-35

5.3. Model

The process flow diagram of the model used to do the cycle calculations is displayed in figure 5.2. The absorber and condenser exchange heat with the seawater and the high pressure generator uses the heat from the exhaust gas from the Diesel engine to evaporate ammonia from the solution. The ionic liquid [Bmim][BF4] is used as absorbent as this ionic liquid performed best in previous research. The equations and the calculation procedure of the cycle are described in chapter 3.

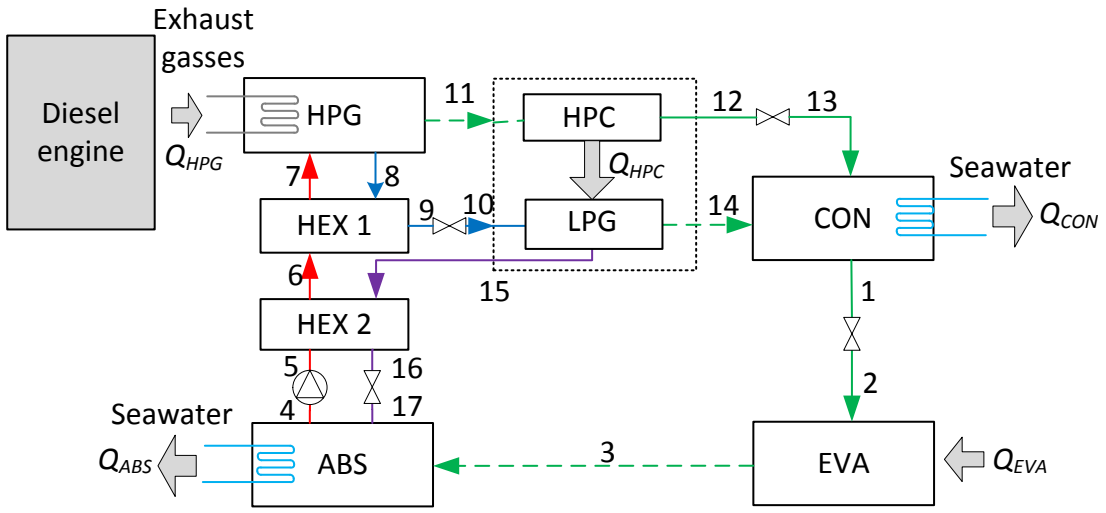

Figure 5.2: Process flow diagram of the double-effect absorption cycle in a series configuration. The red, blue and purple lines indicate the solution of the weak, intermediate and strong concentration. Green lines indicate the refrigerant flows. The dotted lines indicate the vapor phase and the solid lines indicate the liquid phase. The grey arrows indicate where the exhange of heat takes place.

5.4. Results

5.4.1. Cooling power potential

The fishing vessel is equipped with a 7920 kW Wartsila Diesel engine. The high temperature heat stored in the exhaust gas from this engine can be used as input power for absorption refrigeration. Depending on the operating mode, the engine runs at different loads. The temperature and the mass flow of the flue gas are dependent on the load of the engine. Table 5.3 lists the properties of the exhaust gas for different engine loads over the period of a year. The majority of the time the vessel operates at 90 % load during which it has a significant higher exhaust gas mass flow than at lower loads and thus more recoverable heat. To prevent risk of sulfur corrosion, the exhaust gas cannot be cooled down below 167 °C [28]. In the high pressure generator a pinch temperature of 10 K is assumed which means that T_7 will always be higher than 157 °C.

Equation 5.1 is used to calculate the recoverable heat from the flue gas. The amount of heat that can be extracted to power the double-effect absorption cycle depends on how much the exhaust gas flow can be cooled down. By increasing T_8, T_7 will also increase so the exhaust gas has a smaller temperature range over which it can be cooled. At the same time, by increasing T_8, the COP of the cycle increases until it reaches its maximum. This means that for every engine load and seawater temperature there is an optimum high pressure generator solution outlet temperature (T_8) for which the potential cooling power is at its highest.

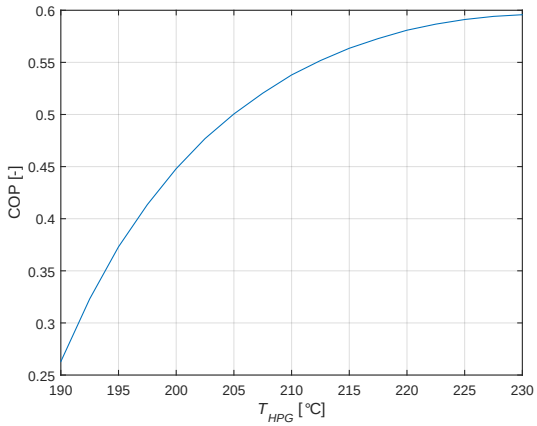

(a) The influence of T_{HPG} on the COP of the cycle.

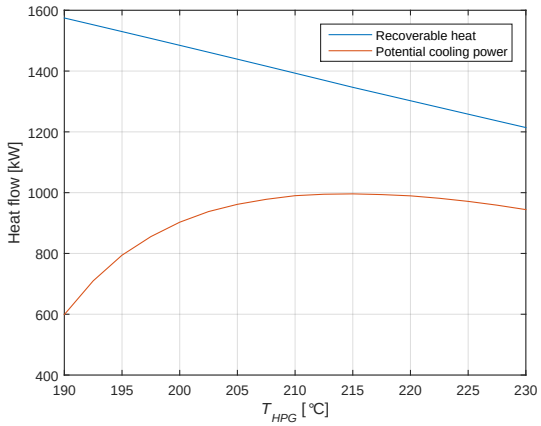

(b) The influence of T_{HPG} on the heat flows.

Figure 5.3: The performance and potential of the double-effect absorption cycle using [Bmim][BF4] and ammonia as working pair. For the conditions T_{EVA} = -6 °C and T_{CON}=T_{ABS}=37°C. This corresponds to a seawater temperature of 32°C. The recoverable heat shows a negative trend with increasing T_{HPG} and the potential cooling power shows a maximum at around 215 °C. Not all conditions are possible, T_7 must always be higher than 157 °C

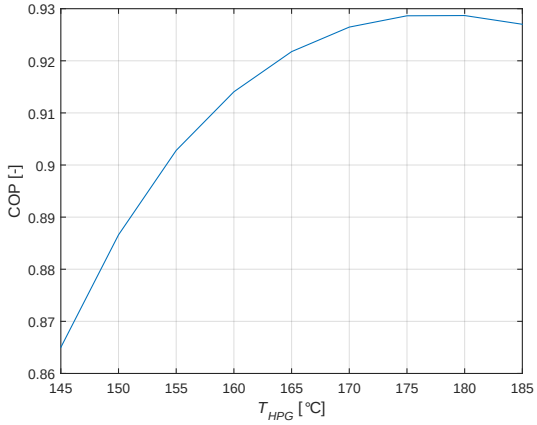

(a) The influence of T_{HPG} on the COP of the cycle.

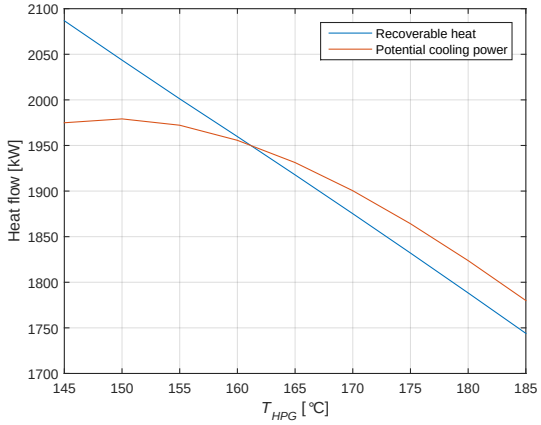

(b) The influence of T_{HPG} on the heat flows.

Figure 5.4: The performance and potential of the double-effect absorption cycle using [Bmim][BF4] and ammonia as working pair. For the conditions: T_{EVA} = -6 °C and T_{CON}=T_{ABS}=21°C. This corresponds to a seawater temperature of 16°C. As expected, the COP and the potential cooling power are much higher compared to tropical seawater temperatures. For some conditions the potential cooling power is higher than the recoverable heat from the exhaust gas. Not all conditions are possible, T_7 must be higher than 157 °C

Table 5.3: Properties of the flue gas coming from the 7920 kW Wartsila Diesel engine. The properties are shown for different engine loads and operating modes for a period of 1 year. The vast majority of the time the engine operates at a load of 90 %.

Engine load	Duration [h]	Exhaust gas flow [kg/s]	Temperature [°C]	Operating mode
90 %	5400	9.35	350	Fishing with production
90 %	400	9.35	350	Fishing without production
70 %	320	7.58	356.5	Sailing to fishing zone, tracking down fish
35 %	1200	4.57	365	Retrieving or placing nets, pumping fish on board
0 %	1440	N/A	N/A	Out of order or unloading fish

$$\dot{Q}_{rec} = c_{p,ex}\dot{m}_{ex}(T_{ex} - (T_7 + 10K)) \tag{5.1}$$

Figure 5.3 shows the COP, the recoverable heat and the potential cooling power as a function of the high pressure generator outlet solution temperature for a seawater temperature of 32 °C (so T_{CON}=T_{ABS}=37°C) and an engine load of 90 %. An optimum for the potential cooling power can be seen around 215 °C. The exhaust heat flow shows a negative linear trend because T_7 increases linearly with T_8. For higher temperatures, the COP stagnates so increasing T_8 more will only negatively affect the potential cooling power. When choosing the optimal temperature for T_8, one always has to check if T_7 is not below 157 °C.

Figure 5.3 shows the performance of the cycle for a seawater temperature of 16 °C. It is clear to see that having a lower temperature for the high pressure generator solution outlet is favorable. However, this would result in the risk of sulfur condensation.

The potential cooling power for the different engine loads and seawater temperatures are listed in table 5.4 and table 5.5. The data is given for seawater temperatures of 16 °C and 32 °C because the documentation of the studied fishing ship uses these conditions. The potential cooling power at lower seawater temperatures is much higher. This large difference can be explained by three reasons. When the seawater temperature is lower, the absorber and condenser operate at a lower temperature. As explained in chapter 2, having a lower absorber and condenser temperature increases the COP of the cycle so more recovered heat from the exhaust gas can be converted into cooling power. Additionally, the optimal high pressure generator solution outlet temperature is much lower for lower seawater temperatures. This means that the exhaust gas can be cooled down more resulting in more recoverable heat. Furthermore, the pump power at lower seawater temperatures is much lower because the pressure difference between the absorber and the high pressure generator is much lower. For lower seawater temperatures, the potential cooling power would be even higher if the absorption cycle would run at lower temperatures but this would violate the minimum exhaust gas temperature for the prevention of sulfur corrosion.

The results show that for an engine load of 90 % and a seawater temperature of 16 °C the absorption cycle can supply the cooling demand for the entire chilled water plant, almost 27 % of the total cooling demand. However, for higher seawater temperatures and lower engine loads, a back-up cooling system or another heat source is needed to power the absorption cycle.

Table 5.4: The cooling power potential of the double-effect absorption cycle. Using waste heat of a 7920 kW Wartsila Diesel engine at a seawater temperature of 16°C for different engine loads.

Seawater temperature of 16 °C			
Engine load	90 %	70 %	35 %
Potential cooling power [kW]	1871.6	1571.4	990.0516
Recoverable heat [kW]	1840.7	1545.5	973.7268
Pump power	175.4787	147.33	92.8265
COP [-]	0.9283	0.9283	0.9283
T_{EVA} [°C]	-6	-6	-6
$T_{CON} = T_{ABS}$ [°C]	21	21	21
T_8 [°C]	174	174	174
T_7 [°C]	157.71	157.7136	157.7136
Inlet Temperature exhaust gas [°C]	350	356.5	365
Outlet Temperature exhaust gas [°C]	167.71	167.71	167.71

Table 5.5: The cooling power potential of the double-effect absorption cycle. Using waste heat of a 7920 kW Wartsila Diesel engine at a seawater temperature of 32°C for different engine loads.

Seawater temperature of 32 °C			
Engine load	90 %	70 %	35 %
Potential cooling power [kW]	995.28	842.618	539.89
Recoverable heat [kW]	1346.5	1109.09	710.596
Pump power [kW]	420.62	341.5712	218.855
COP [-]	0.5632	0.5809	0.5809
T_{EVA} [°C]	-6	-6	-6
$T_{CON} = T_{ABS}$ [°C]	37	37	37
T_8 [°C]	215	220	220
T_7[°C]	206.65	211.03	211.03
Inlet Temperature exhaust gas [°C]	350	356.5	365
Outlet Temperature exhaust gas [°C]	216.65	221.03	221.03

5.4.2. Influence of seawater temperature

The seawater temperature will vary depending on the location of the vessel. As mentioned before, the seawater temperature has a very strong influence on the performance. Figure 5.5a shows the COP of the cycle as a function of the seawater temperature. The COP shows a strong decrease with increasing seawater temperature. This means that the vessel can save more energy when fishing in a cooler climate.

Figure 5.5b shows the potential cooling power and the recoverable heat from the exhaust gas as a function of the seawater temperature. Both show a strong decrease with increasing seawater temperature. However, for a seawater temperature of 35 °C the cycle could still provide the cooling demand of one of the screw compressors (880kW) used for the chilled water plant.

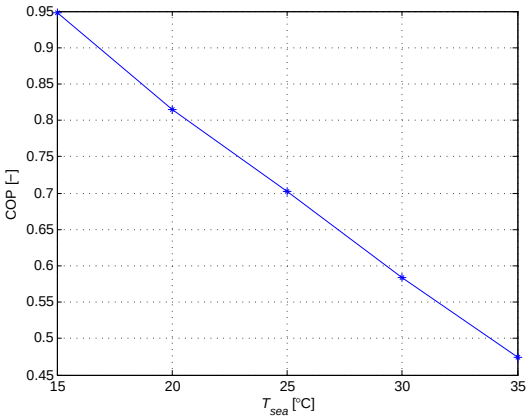

(a) The influence of T_{sea} on the COP of the cycle.

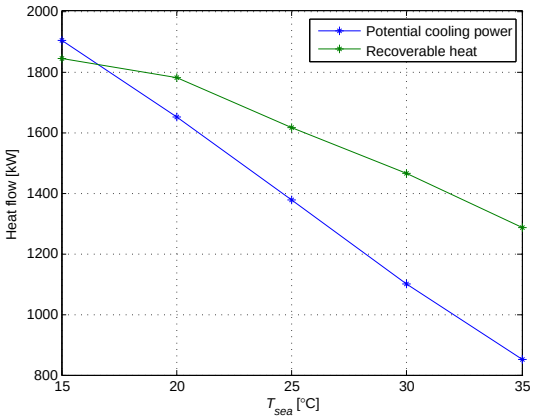

(b) The influence of T_{sea} on the heat flows.

Figure 5.5: The performance and heat flows of the double-effect absorption cycle using [Bmim][BF4] and ammonia as working pair. For the condition T_{EVA} = -6 °C. The recoverable heat and the potential cooling power show a negative trend with increasing T_{sea}. For seawater temperatures above 35 °C the double-effect absorption cycle cannot provide enough cooling power (880 kW) to replace one of the screw compressors.

5.5. Conclusions and recommendations

In this chapter the suitability of absorption refrigeration for the cooling of fish on a fishing vessel is investigated. The thermodynamic model described in chapter 3 uses the heat stored in the exhaust gas coming from the Diesel engine of the vessel and converts it to cooling power. With this model, the potential cooling power that the double-effect effect absorption refrigeration cycle using ammonia and [Bmim][BF4] as working pair can supply for two different climates has been calculated. The influence of the high pressure generator operating temperature and the seawater temperature on the performance on the cycle is described.

5.5.1. Conclusions

- The double-effect effect absorption refrigeration cycle using ammonia and [Bmim][BF4] as working pair can supply the needed cooling power for the entire chilled water plant for a engine load of 90 % and when the seawater temperature is 16 °C. However, for certain conditions, the cooling power from the existing refrigeration plant is still needed. Hence, the cycle should be used as an auxiliary refrigeration plant, where the screw compressors can be turned off during the right conditions.
- The seawater temperature has a very strong effect on the performance of the cycle, and thus the amount of energy that can be saved. When the seawater temperature increases with 20 K, the amount of potential cooling power decreases with approximately 50 %.

5.5.2. Recommendations

- In order to give an accurate estimation of how much energy can be saved during a year, data of the variation of the seawater temperature during a journey of the vessel is needed.
- The influence of vessel movements and vibrations on the performance of the cycle should be investigated.
- The corrosive effect of seawater on the heat exchangers and the power needed to pump the

seawater through them should be investigated.

- The size and cost of the double-effect absorption cycle on the vessel should be evaluated.
- A dynamic study should be done.

6

Conclusions and outlook

Firstly, a thermodynamic model of a double-effect absorption cycle in series configuration was used to predict the performance and suitability of the ammonia and water working pair. The effect of the operating conditions, design parameters and the influence of the rectifiers needed to purify the refrigerant was investigated. To predict the performance of nine ionic liquids as absorbents, their vapor-liquid equilibrium and enthalpy, derived from heat capacities, were correlated using experimental data. With the correlations and the thermodynamic model of the double-effect absorption cycle in series configuration, the performance and suitability of these new working pairs were investigated. However, in order to give accurate predictions of the performance of the ionic liquids, excess enthalpy data is needed. Thus, a method to measure the excess enthalpy of these working pairs was proposed. Lastly, the potential of using the ionic liquid [Bmim][BF4] and ammonia as working pair in double-effect absorption cycles on board of a fishing vessel for the refrigeration of fish was studied.

6.1. Conclusions

- For the investigated operating conditions, the ionic liquids [Bmim][BF4], [Mmim][DMP] and [Emim][SCN] used as absorbents in the double-effect absorption cycle reached the best performance.

- Ammonia and the best performing ionic liquids show promise as a potential working pair for the double-effect cycle in series configuration. For an evaporation temperature of 0 °C and when a high temperature heat source is available, the proposed working pairs perform better than ammonia and water in the double-effect cycle.

- For evaporation temperatures above 0 °C, ammonia based cycles are not as good as the ones that use water as refrigerant.

- The refrigeration of fish on fishing vessels could be a promising application for the double-effect absorption refrigeration cycle using ammonia and ionic liquids as working pairs. For an engine load of 90 % and a seawater temperature of 16 °C, 27 % of the entire cooling demand needed by a large trawler fishing vessel could be supplied by absorption refrigeration.

6.2. Outlook

- In order to give accurate predictions of the performance of the investigated ionic liquid absorbents using ammonia as refrigerant, experimental data of the mixing enthalpy of the ammonia and ionic liquid working pairs is needed and the effect of the viscosity on the performance of the cycle should be investigated. Ionic liquid and ammonia working pairs have never been used in an actual experimental absorption cycle set-up. This would be the next big step towards the realization of actual functional absorption cycles using this new working pair.
- Absorption refrigeration on fishing vessels has potential but many challenges exist. Not much is known about the influence of movements and vibrations of the vessel on the performance of absorption refrigeration cycles. Additionally, because space on a ship is limited, the required dimensions of the system have to be evaluated and an estimation of the investment costs should be made.

Bibliography

[1] E. Abumandour, F. Mutelet, and D. Alonso. Performance of an absorption heat transformer using new working binary systems composed of ionic liquid and water. *Applied Thermal Engineering*, 94:579–589, 2016. ISSN 13594311. doi: 10.1016/j.applthermaleng.2015.10.107.

[2] M. Azhar and M. Siddiqui. Energy and exergy analyses for optimization of the operating temperatures in double effect absorption cycle. *Energy Procedia*, 109:211 – 218, 2017. ISSN 1876-6102. doi: https://doi.org/10.1016/j.egypro.2017.03.043. URL `http://www.sciencedirect.com/science/article/pii/S1876610217300656`. International Conference on Recent Advancement in Air Conditioning and Refrigeration, {RAAR} 2016, 10-12 November 2016, Bhubaneswar, India.

[3] F. Billiard. The Kyoto Protocol. *Bulletin de Institute International du Froid*, 1990.

[4] W. Cai, M. Sen, and S. Paolucci. Dynamic Modeling of an Absorption Refrigeration System Using Ionic Liquids. In *Proceedings of 2007 ASME International Mechanical Engineering Congress and Exposition*, pages 227–236, Seattle, Washington, USA, 2007. American Society of Mechanical Engineers.

[5] Y. Cao and T. Mu. Comprehensive Investigation on the Thermal Stability of 66 Ionic Liquids by Thermogravimetric Analysis). *Ind. Eng. Chem. Res*, 53(20):8651–8664, 2014.

[6] W. Chen and S. Liang. Thermodynamic analysis of absorption heat transformers using [mmim]DMP/H2O and [mmim]DMP/CH3OH as working fluids. *Applied Thermal Engineering*, 99:846–856, 2016. ISSN 13594311. doi: 10.1016/j.applthermaleng.2016.01.135.

[7] Y. Chen, Y. Cao, Y. Shi, Z. Xue, and T. Mu. Quantitative Research on the Vaporization and Decomposition of [EMIM][Tf2N] by Thermogravimetric Analysis Mass Spectrometry. *Ind. Eng. Chem. Res.*, 51(21):7418–7427, 2012.

[8] Y. Chen, W. Han, and H. Jin. Thermodynamic performance optimization of the absorption-generation process in an absorption refrigeration cycle. *Energy Conversion and Management*, 126:290 – 301, 2016. ISSN 0196-8904. doi: https://doi.org/10.1016/j.enconman.2016.07.086. URL `http://www.sciencedirect.com/science/article/pii/S0196890416306641`.

[9] L. Dong, D. Zheng, N. Nie, and Y. Li. Performance prediction of absorption refrigeration cycle based on the measurements of vapor pressure and heat capacity of H2O+[DMIM]DMP system. *Applied Energy*, 98:326–332, 2012. ISSN 03062619. doi: 10.1016/j.apenergy.2012.03.044.

[10] V. Eyringer, H.W. Kohler, and A. Lauer. Emissions from international shipping: 2. Impact of future technologies on scenarios until 2050. *Journal of geophysical research*, 2005. doi: 10.1016/j.enconman.2014.04.077.

[11] Z. Fang, R.L. Smith, and X. Qi. *Production of Biofuels and Chemicals with Ionic Liquids*. Springer, 2014. ISBN 9789400777101.

[12] Z. He, Z. Zhao, X. Zhang, and H. Feng. Thermodynamic properties of new heat pump working pairs: 1,3-Dimethylimidazolium dimethylphosphate and water, ethanol and methanol. *Fluid Phase Equilibria*, 298(1):83–91, nov 2010. ISSN 03783812. doi: 10.1016/j.fluid.2010.07.005.

[13] K.E. Herold, R. Radermacher, and S.A. Klein. *Absorption Chillers and Heat Pumps*. CRC Press, 1996. ISBN 9780849394270.

[14] J.G. Kabo, A.V. Blokhin, Y.U. Paulechka, A.G Kabo, M.P. Shymanovich, and J.W. Magee. Thermodynamic Properties of 1-Butyl-3-methylimidazolium Hexafluorophosphate in the Condensed State. *Journal of Chemical & Engineering Data*, 49(3):453–461, 2004. ISSN 0021-9568.

[15] D.S. Kim and C.A. Infante Ferreira. Solar refrigeration options a state of the art review. *International Journal of Refrigeration*, 31(1):3–15, 2008. ISSN 01407007.

[16] A.A. Kiss and C.A. Infante Ferreira. *Heat Pumps in Chemical Process Industry*. CRC Press, 2016. ISBN 9781498718950.

[17] E. Lemmon, M.L. Huber, and M.O. McLinden. NIST Reference fluid thermodynamic and transport properties, 2013.

[18] G. Li, Q. Zhou, X. Zhang, S. Zhang, and J. Li. Solubilities of ammonia in basic imidazolium ionic liquids. *Fluid Phase Equilibria*, 297(1):34–39, 2010. ISSN 03783812.

[19] D. Matkowska and T. Hofman. High-pressure volumetric properties of ionic liquids: 1-butyl-3-methylimidazolium tetrafluoroborate, [C4mim][BF4], 1-butyl-3-methylimidazolium methylsulfate [C4mim][MeSO4] and 1-ethyl-3-methylimidazolium ethylsulfate, [C2mim][EtSO4]. *Journal of Molecular Liquids*, 165:161–167, 2012.

[20] MATLAB. *version 7.10.0 (R2010a)*. The MathWorks Inc., Natick, Massachusetts, 2010.

[21] P. Navarro, M. Larriba, E. Rojo, J. Garca, and F. Rodriguez. Thermal Properties of Cyano-Based Ionic Liquids. *Journal of Chemical & Engineering Data*, 58(8):2187–2193, 2013. ISSN 0021-9568.

[22] US Secretary of Commerce on behalf of the United States of America. Ionic Liquids Database - ILThermo (v2.0), 2017. URL `http://ilthermo.boulder.nist.gov/`.

[23] K. Paduszyski, M. Krolikowski, and U. Domanska. Excess enthalpies of mixing of piperidinium ionic liquids with short-chain alcohols: Measurements and PC-SAFT modeling. *Journal of Physical Chemistry B*, pages 3–8, 2016. ISSN 03783812.

[24] Y. U. Paulechka, A. V. Blokhin, G. J. Kabo, and A. A. Strechan. Thermodynamic properties and polymorphism of 1-alkyl-3-methylimidazolium bis(triflamides). *Journal of Chemical Thermodynamics*, 39(6):866–877, 2007. ISSN 00219614.

[25] Y.U. Paulechka, A.V. Blokhin, and G.J. Kabo. Evaluation of thermodynamic properties for non-crystallizable ionic liquids. *Thermochimica Acta*, 604:122–128, 2015. ISSN 00406031.

[26] M. Pons, F. Meunier, G. Cacciola, R.E. Critoph, M. Groll, L. Puigjaner, B. Spinner, and F. Ziegler. Thermodynamic based comparison of sorption systems for cooling and heat pumping. *International Journal of Refrigeration*, 25:5–17, 1999.

[27] J. Ren, Z. Zhao, and X. Zhang. Vapor pressures, excess enthalpies, and specific heat capacities of the binary working pairs containing the ionic liquid 1-ethyl-3-methylimidazolium dimethylphosphate. *The Journal of Chemical Thermodynamics*, 43(4):576–583, 2011. ISSN 00219614.

[28] W. Salmi, J. Vanttola, M. Elg, and M. Kuosa. Using waste heat of ship as energy source for an absorption refrigeration system. *Applied Thermal Engineering*, 115:501–516, 2017. ISSN 13594311. doi: 10.1016/j.applthermaleng.2016.12.131. URL `http://linkinghub.elsevier.com/retrieve/pii/S135943111634443X`.

[29] M. B. Shiflett and A. Yokozeki. Solubility and diffusivity of hydrofluorocarbons in room-temperature ionic liquids. *AIChE Journal*, 52(3):1205–1219, 2006. ISSN 0001-1541. doi: 10.1002/aic.10685.

[30] A. Sozen, D. Altiparmak, and H. Usta. Development and testing of a prototype of absorption heat pump system operated by solar energy. *Applied Thermal Engineering*, 22(16):1847–1859, 2002. ISSN 13594311.

[31] G. Sun, D. Zheng, W. Huang, and L. Dong. The measurement of ammonia solubility in the ionic liquid 1, 3-dimethylimidazolium dimethylphosphate ([Dmim] DMP). *Journal of Beijing University of Chemical Technology (Natural Science Edition)*, 39(4):17–21, 2012.

[32] D. Waliszewski. Heat capacities of the mixtures of ionic liquids with methanol at temperatures from 283.15K to 323.15K. *The Journal of Chemical Thermodynamics*, 40(2):203–207, 2008. ISSN 00219614. doi: 10.1016/j.jct.2007.07.001.

[33] M. Wang and C.A. Infante Ferreira. Absorption heat pump cycles with ammonia ioniq liquid working pairs. 2017.

[34] P. Wasserscheid and T. Welton. *Ionic Liquids in Synthesis*. Wiley, 2008. ISBN 9783527621194.

[35] Z.Y. Xu and R.Z. Wang. Absorption refrigeration cycles: Categorized based on the cycle construction. *International Journal of Refrigeration*, 62:114 – 136, 2016. ISSN 0140-7007. doi: https://doi.org/10.1016/j.ijrefrig.2015.10.007. URL `http://www.sciencedirect.com/science/article/pii/S0140700715003011`.

[36] A. Yokozeki and M.B. Shiflett. Vaporliquid equilibria of ammonia+ionic liquid mixtures. *Applied Energy*, 84(12):1258–1273, 2007. ISSN 03062619.

[37] A. Yokozeki and M.B. Shiflett. Ammonia Solubilities in Room-Temperature Ionic Liquids. *Industrial & Engineering Chemistry Research*, 46(5):1605–1610, 2007. ISSN 0888-5885.

[38] Y.H. Yu, A.N. Soriano, and M.H. Li. Heat capacities and electrical conductivities of 1-ethyl-3-methylimidazolium-based ionic liquids. *Journal of Chemical Thermodynamics*, 41(1):103–108, 2009. ISSN 00219614.

[39] D. Zheng, L. Dong, W. Huang, X. Wu, and N. Nie. A review of imidazolium ionic liquids research and development towards working pair of absorption cycle. *Renewable and Sustainable Energy Reviews*, 37:47–68, 2014. ISSN 13640321.

[40] F. Ziegler. State of the art in sorption heat pumping and cooling technologies. *International Journal of Refrigeration*, 25(25):450–459, 1990.